

1 **Petrological and Geochemical Variation during the Soufrière Hills Eruption (1995-2010)**

2  
3 Thomas E. Christopher <sup>1\*</sup>, Madeleine C. S. Humphreys <sup>2,3</sup>, Jenni Barclay <sup>4</sup>, Kimberly Genareau <sup>5</sup>, Sarah  
4 M.H. De Angelis <sup>6</sup>, Melissa Plail <sup>4</sup>, Amy Donovan <sup>7</sup>

5  
6 1 Montserrat Volcano Observatory, Salem, Montserrat, West Indies.

7 2 Earth Sciences Department, University of Oxford, South Parks Road, Oxford OX1 3AN, UK.

8 3 Present address: Department of Earth Sciences, Durham University, Science Labs, Durham, DH1 3LE,  
9 UK

10 4 School of Environmental Sciences, University of East Anglia, Norwich NR9 7TJ, UK.

11 5 Department of Earth and Environmental Sciences, Lehigh University, 1 West Packer Avenue  
12 Bethlehem, PA 18015-3001 USA

13 6 Geophysical Institute, University of Alaska Fairbanks, 903 Koyukuk Drive, P.O. Box 757320,  
14 Fairbanks, AK

15 7 Department of Geography, University of Cambridge, Downing Place, Cambridge CB2 3EN

16  
17 \*corresponding author; [Thomas@mvo.ms](mailto:Thomas@mvo.ms)

18  
19 Words = 11744 References = 101 Tables = 16 Figures = 11

20  
21 Abbreviated Title: Petrological and Geochemical variation

22 **ABSTRACT**

23 The andesite lava erupted at the Soufrière Hills Volcano is crystal rich with 33-63% phenocrysts, of  
24 plagioclase (65%); amphibole (28%), orthopyroxene (7%) and minor Fe-Ti oxide and clinopyroxene  
25 microphenocrysts. The andesite hosts mafic enclaves which have similar mineral phases to the andesite.  
26 The enclaves are generally crystal poor but can have up to 27% of inherited phenocrysts from the  
27 andesite, the majority of which are plagioclase. The eruption is defined by discrete periods of extrusion  
28 called phases, separated by pauses. The enclaves exhibit bulk geochemical trends that are consistent with  
29 fractionation. We infer that the intruded mafic liquids of Phases I and II interacted and assimilated  
30 plutonic residue remaining from the multiple prior mafic intrusions, while the basaltic liquids from Phases  
31 III and V assimilated relatively little material. We also infer a change in the basaltic composition coming  
32 from depth. The bulk Fe contents of both magma types are coupled and they both show a systematic inter-  
33 phase variation in Fe content. We interpret the coupled Fe variation to be due to contamination of the  
34 andesite from the intruding basalt via diffusion and advection processes, resulting in the erupted andesite  
35 products bearing the geochemical imprint of the syn-eruptive enclaves.

36

37 The Soufrière Hills volcano is an andesitic dome complex located on the island of Montserrat in the  
38 Lesser Antilles arc. The present eruption began on the evening of July 18<sup>th</sup> 1995 with ash venting  
39 followed by phreatic explosions over the next weeks and months (Young et al., 1998; Robertson et al.,  
40 2000). Juvenile material arrived at the surface around November 15<sup>th</sup> 1995 (Young et al., 1998) building  
41 the first lava dome of the eruption. Lava extrusion and dome growth at Soufrière Hills volcano has not  
42 been continuous during the eruption; dome growth has been defined by distinct periods of extrusion  
43 referred to as 'phases' separated by periods of no activity, referred to as 'pauses'. Each period of  
44 extrusion was volcanologically unique, however each of the effusive phases were punctuated by  
45 pyroclastic flows generated by dome collapse or Vulcanian explosions.

46

47 Phase I of dome growth (mid November 1995 to mid March 1998) was characterized by cyclic growth  
48 and frequent collapse of the lava dome, with a mean extrusion rate of  $4.5 \text{ m}^3 \text{ s}^{-1}$  (Wadge et al., 2010)  
49 which peaked at about  $10 \text{ m}^3 \text{ s}^{-1}$  (Herd et al., 2005). The volcanic activity of Phase I is described in detail  
50 elsewhere (e.g. Aspinall et al., 1998; Young et al., 1998; Miller et al., 1998; Calder et al., 2002; Norton et  
51 al., 2002). The cessation of lava extrusion in March 1998 occurred when a dome with a volume of  $113 \times$   
52  $10^6 \text{ m}^3$  was present in the crater (Norton et al., 2002).

53

54 Phase II (mid November 1999 to mid July 2003), showed a less variable extrusion rate with a mean of  $2.9$   
55  $\text{m}^3 \text{ s}^{-1}$  (Wadge et al., 2010), peaking at about  $4 \text{ m}^3 \text{ s}^{-1}$  (Herd et al., 2005). This resulted in the construction  
56 of a larger volume dome than any extruded during Phase I. Dome collapses were less frequent than during  
57 Phase I but involved larger volumes, culminating in the largest volume collapse of the eruption to date in  
58 July 2003. This removed almost the entire volume of the dome ( $\sim 200 \times 10^6 \text{ m}^3$  Edmonds et al., 2006). The  
59 ensuing period of pause lasted 24 months, four months longer than the first pause and to date is the only  
60 prolonged period of the eruption with a relatively dome-free crater.

61

62 Phase III (early August 2005 to early April 2007), started slowly and the growth rate for most of August  
63 was slow and steady ( $0.5\text{-}0.7 \text{ m}^3/\text{s}$ ). Low extrusion rates continued through December and January ( $3.2\text{-}$   
64  $3.9 \text{ m}^3/\text{s}$ ), but the extrusion rate exceeded  $10 \text{ m}^3 \text{ s}^{-1}$  in February 2006 and remained high for the rest of the  
65 extrusive episode. The dome collapse event on the morning of May 20<sup>th</sup> 2006 involved  $\sim 100 \times 10^6 \text{ m}^3$  of  
66 dome material and emptied the crater; however an observation flight later that day revealed new extrusion  
67 in the vent area. Subsequent growth continued until extrusive activity stopped in April 2007 leaving a  
68 dome of  $\sim 200 \times 10^6 \text{ m}^3$  in the crater. This was the largest dome present during any pause for the current  
69 eruption. Phase III was characterized by much less pyroclastic flow activity; to such an extent that the  
70 first flow large enough to reach the sea occurred on the morning of May 20<sup>th</sup> 2006.

71

72  
73  
74  
75  
76  
77  
78  
79  
80  
81  
82  
83  
84  
85  
86  
87  
88  
89  
90  
91

*Phases IV and V volcanic activity*

The first three phases of extrusion were characterized by extended periods (on the order of years) of lava production separated by pauses of similar lengths. This was not the case for Phases IV and V. Phase IV was characterized by two separate episodes of extrusion punctuated by explosions, the first episode was in July-August 2008 and the second in December 2008-January 2009. The first episode of Phase IV started with a Vulcanian explosion on July 28<sup>th</sup> 2008 while the December 2008- January 2009 episode started and ended with Vulcanian explosions on December 3<sup>rd</sup> 2008 and Jan 3<sup>rd</sup> 2009 respectively. An approximate volume of  $39 \times 10^6 \text{ m}^3$  of andesite was extruded for Phase IV (Wadge et al., 2010). Phase V was also short lived (early October 2009 till mid February 2010), and extruded  $\sim 74 \times 10^6 \text{ m}^3$ . As was the case with Phase IV, Phase V produced a high occurrence of explosive activity (Stinton et al., this volume). The extrusion was also cyclic and the cycles were characterized by periods of intense pyroclastic flow generation which would wax and wane on time scales ranging from 4 to 13 hours (Odbert et al., this volume). The textures present in the Phase IV and Phase V products are similar to that noticed in Phases I, II and III. There however seems to be an increase in the vesicularity of the andesite products with friable hand specimens being more commonplace in Phases IV and V. The presence of banded pumice in the July 28<sup>th</sup> 2008 explosion products was a new occurrence in the eruption.

*Aim of Current Work*

The initial extrusive episode, Phase I received considerable attention with regards to the petrological and geochemical characteristics of the eruptive products (e.g. Barclay et al., 1998; Devine et al., 1998a; 1998b; Murphy et al., 1998; Murphy et al., 2000; Higgins & Roberge, 2003; Zellmer et al., 2003a; 2003b). The initial research was focused on constraining pre-eruptive storage conditions of the erupted

97 andesite (e.g. Barclay et al., 1998; Couch et al., 2003a; Rutherford & Devine, 2003) as well as  
98 establishing the role of the intruding mafic magma in the onset and fueling of the eruption (e.g. Murphy  
99 et al., 1998; Murphy et al., 2000; Devine et al., 2003). Long lived eruptions (such as the eruption at  
100 Arenal volcano, Reagan et al., 1987) can produce products with temporal variations in chemistry and  
101 mineralogy, which may provide useful data for unlocking processes responsible for driving such  
102 eruptions (e.g. Streck et al., 2002; Bolge et al., 2006; Ryder et al., 2006).

103  
104 The preliminary research has without doubt provided valuable information about the processes  
105 responsible for triggering and driving the eruption and hence influencing the eruption style. However the  
106 ongoing nature of the eruption now provides an opportunity to address any temporal variations in textures  
107 and chemistry of the minerals as well as the bulk rock compositions that may have occurred as the  
108 eruption proceeded. The aim of this publication is to present a holistic overview of geochemical and  
109 petrological data collected from the enclaves and host andesite throughout the current Soufrière Hills  
110 eruption. The Phase IV and Phase V products are compared to the earlier products, highlighting any  
111 temporal variations present and their bearing on magma chamber and eruption processes. In particular, we  
112 focus on temporal variations in bulk rock FeO, and propose that this is linked to similar compositional  
113 variations in some mineral phases. We also make a brief comparison to the Mt Pelée products where the  
114 processes responsible for generating the andesitic compositions are well constrained (e.g. Dupuy et al.,  
115 1985; Fichaut et al., 1989a; Pichavant et al., 2002).

116

## 117 **ANALYTICAL TECHNIQUES**

### 118 *Microprobe Analysis*

119 Samples from Phase IV were analyzed using a Cameca 5-spectrometer SX-100 instrument at the  
120 Department of Earth Sciences University of Cambridge. Minerals were analyzed using a 2  $\mu\text{m}$ , 15 kV, 10

121 nA beam for major elements and a 100 nA beam for minor and trace elements. Glasses were analyzed  
122 using a 10 µm, 15 kV, 2 nA beam to avoid alkali migration (Devine et al., 1995; Humphreys et al., 2006),  
123 with a 10 nA beam for minor and trace elements (e.g. Cl, Ti, Mg).

124 The Phase V minerals were probed using a JEOL8600 four spectrometer instrument at the Research  
125 Laboratory for Archaeology & the History of Art, University of Oxford. Minerals were analyzed with a  
126 15 keV, 15 nA, 1 micron beam. Peak analysis count times were 30s, except for Na (20s) and Cl (40s).  
127 Glass analysis was carried out with a 15 keV, 6 nA, 10 µm diameter beam. Peak count times for all  
128 elements were 30s, except for Na (10s), Cl (40s) and P (60s). Amphibole structural formulae were  
129 recalculated on the basis of 23 O atoms following Schumacher (1997) and oxide minerals using Stormer  
130 (1983).

131

### 132 *Bulk Rock Analysis*

133 Andesite and enclave XRF data from Phase II along with some Phase III andesites were obtained by the  
134 MVO with the analyses performed at the University of Leicester labs under MVO contract. This is the  
135 same laboratory that produced the Phase I data presented in Murphy et al. (2000) and Zellmer et al.  
136 (2003a). The remaining andesite bulk rock data from Phase III and all of Phases IV and V were obtained  
137 from the University of East Anglia under MVO contract. Enclave bulk rock data from Phase III onwards  
138 was also obtained from the University of East Anglia under MVO contract. Bulk enclave data from Phase  
139 II were from two sources, the first being McGill University in Canada and the second from the British  
140 Geological Survey (BGS) labs in Nottingham England. Detailed information about lab, instrumentation  
141 and samples analyzed by each lab is presented in Table 1. Bulk rock data is unavailable for Phase IV  
142 enclaves due to the limited volume of observed basaltic material (mm size inclusions) extruded and the  
143 lack of extensive deposits available for sampling. Microprobe glass and mineral chemistry data were  
144 however obtained from mafic fragments in some thin sections.

145

146 **PREVIOUS WORK**

147 Andesite and enclave bulk rock XRF analyses of Phase I major and trace elements were compiled from  
148 the literature (Devine et al., 1998a; Murphy et al., 1998; Murphy et al., 2000; Zellmer et al., 2003a).  
149 Previous petrological studies on the eruption products of Phases I, II and III, are present in a variety of  
150 sources including Barclay et al. (1998), Devine et al. (1998b), Murphy et al. (2000), Couch et al. (2003a;  
151 2003b), Zellmer et al. (2003a), Humphreys et al. (2009a; 2009b), Barclay et al. (2010) Humphreys et al.  
152 (2010). Here we summarize the Phase I bulk rock and petrological characteristics of the Phase I, II and  
153 III products from the literature.

154

155 *Andesite Textures*

156 Samples are generally crystal-rich (33-63 vol% phenocrysts), with a phenocryst assemblage dominated by  
157 plagioclase (64-78% of phenocrysts) complemented by lesser amphibole (8-28%), orthopyroxene (3-7%)  
158 and microphenocrysts of Fe-Ti oxides (1.5-3%). Maximum phenocryst sizes are typically ~7 mm for  
159 hornblende, ~3-4 mm for plagioclase and ~5 mm for orthopyroxene. Clinopyroxene microphenocrysts (<  
160 1%) are present, as well as accessory apatite. Quartz is also present as rounded, embayed crystals  
161 sometimes jacketed by clinopyroxene. The variations in modal mineral contents are presented in Table 2.

162

163 The andesite groundmass is generally microcrystalline but can contain up to 25% rhyolitic glass in rapidly  
164 erupted samples. Cristobalite is present in slower erupted dense dome samples and can be up to 15 wt% in  
165 the groundmass, or more commonly as a vapor phase precipitate in the vesicles. The glass is commonly  
166 observed to have undergone phase separation and or devitrification in dome samples. Hornblende is  
167 replaced by orthopyroxene and clinopyroxene, thus yielding a groundmass normally comprising  
168 plagioclase, two pyroxenes and Fe-Ti oxides, with wide variations in microlite textures. No systematic  
169 differences in texture modal proportion or mineral composition have been observed within the andesites  
170 of Phases I, II and III (Table 2).

171

172

173

#### 174 *Enclave Textures*

175 Mafic enclaves have been present in the eruptive products of the Soufrière Hills volcano as far back as  
176 24ka (Wadge & Isaacs, 1988). The enclaves from Phases I, II and III are typically small (< 30cm) with a  
177 maximum reported length of 80 cm (Barclay et al., 2010; Plail et al., this volume); their shapes vary from  
178 ellipsoidal to angular. The ellipsoidal enclaves have smooth or crenulate, chilled contacts with the  
179 andesite. Small mm-scale fragments of enclaves are also observed in the andesite. The enclaves contain  
180 similar mineral phases to that of the andesite; they are however recognized by the higher abundance of  
181 mafic minerals, and a higher abundance of clinopyroxenes relative to orthopyroxene. There are no true  
182 phenocrysts present, but based on chemistry and texture there are andesite-derived xenocrysts of  
183 plagioclase, amphibole and orthopyroxene present in the enclaves.

184

185 The xenocryst contents can be up to 5% by volume for Phase I enclaves (Murphy et al., 1998; 2000), and  
186 up to 27% for Phase III; two thirds of which are normally plagioclase (Plail et al., this volume). The  
187 enclave groundmass is typically fine grained, consisting of randomly oriented interlocking elongate or  
188 acicular crystals of plagioclase, orthopyroxene, clinopyroxene and amphibole forming a diktytaxitic  
189 framework. About ~10% of residual rhyolitic glass with variable amounts of devitrification is observed in  
190 most thin sections, banded textures are also present in some scoriaceous samples.

191

#### 192 *Mineral Textures and Composition – (Andesite and Enclave)*

193

194 Due to their similarities in crystal phases, the initial findings on the mineral compositions of the andesite  
195 and enclaves are both summarized together in this section. A through overview of the mineral chemistry  
196 from the early erupted products is presented in Barclay et al. (1998), Devine et al. (1998a; 1998b) and



197 Murphy et al. (1998; 2000) for Phase I and Humphreys et al. (2009a; 2009b) for the products of Phases II  
198 and III.

199  
200

### 201 *Plagioclase*

202 Plagioclase is present as phenocrysts, microphenocrysts and microlites in the andesite with the  
203 phenocrysts showing a variety of zoning textures (Table 3; see also Murphy et al., 2000; Humphreys et  
204 al., 2009a; 2013). Oscillatory and patchy zoning are common in the phenocryst cores, including the cores  
205 of sieved crystals, which are interpreted to have experienced direct contact with melt of a more mafic  
206 nature. The modal proportion of each plagioclase textural type varies between samples. Plagioclase is  
207 present in the enclaves mostly as microlites, with minor inherited phenocryst from the andesite also  
208 present.

209

210 Plagioclase phenocrysts in the andesite have sodic cores (typically  $An_{48-58}$ , but with calcic zones up to  
211  $An_{80}$ ) with either normal or reversed zoned rims, while the microlites have more calcic cores  $An_{60-75}$  and  
212 can be normally, or to a lesser extent, reversed zoned. The plagioclase microlite cores in the enclaves are  
213 calcic up to  $An_{93}$  and normally zoned. Apart from the differences in anorthite content, the andesite  
214 phenocrysts generally have lower Fe contents than the enclave crystals. Most andesite microlites, some  
215 microphenocrysts and the sieved rims are generally richer in FeO content relative to the phenocryst rims,  
216 their elevated FeO contents are similar to that observed in the enclave plagioclase crystals (Figure 1e & f,  
217 Table 4).

218

### 219 *Amphibole*

220 Amphibole phenocrysts in the andesite show green-brown pleochroism and can show oscillatory zoning  
221 (Rutherford & Devine, 2003; Humphreys et al., 2009b). Amphiboles can have irregular rims (indicating  
222 slight resorption) or pristine rims, but commonly show a variety of breakdown textures, of which three

223 end-members can be identified (summarized from Devine et al., 1998a; Murphy et al., 2000; Rutherford  
224 & Devine, 2003; Buckley et al., 2006; Humphreys et al., 2009b; Plechov et al., 2008):

- 225
- 226 (i) Fine-grained intergrowths of clinopyroxene, orthopyroxene, Fe-Ti oxides and plagioclase, growing  
227 where the amphibole is in contact with melt. This breakdown texture can pseudomorph the original  
228 crystal and is thought to form as a result of decompression during ascent due to changes in  $pH_2O$ .  
229 The development of these rims can be used as an indicator of ascent conditions, with the thicker  
230 rims developing during slower ascent. The rim thicknesses observed in the samples represent ascent  
231 rates of  $> 0.019$  m/s (Devine et al., 1998a; Rutherford & Devine, 2003).
- 232 (ii) Coarser-grained reaction rims dominated by clinopyroxene (preferentially aligned parallel to the c-  
233 axis of the amphibole, and commonly in optical continuity). This rim type can also pseudomorph  
234 the entire crystal and is interpreted as a thermal breakdown texture.
- 235 (iii) Partial to complete opacitisation, particularly along cleavage and cracks or adjacent to vesicles.

236

237 Decompression breakdown rims, thermal breakdown rims and resorbed rims are present in the majority of  
238 analyzed samples; typically a given sample will also show a range of decompression rim thicknesses. In  
239 the mafic enclaves, some amphibole microphenocrysts have undergone partial breakdown or opacitisation  
240 while microlites are normally euhedral and yellowish in appearance. The inherited amphibole phenocrysts  
241 in the enclaves most commonly show thermal breakdown textures. Amphibole compositions in the  
242 andesite range from Mg-hornblende to Mg-hastingsite, with some pargasite present. Amphibole  
243 compositions in the enclaves range from pargasite to Mg-hastingsite. In general, andesite amphibole  
244 phenocrysts have lower  $Al_2O_3$  (6-8 wt%) relative to the enclave amphibole contents of (12-14.5 wt%).

245

246 *Pyroxenes*

247 Orthopyroxene phenocrysts are typically euhedral, although some show slight rounding, which may be  
248 followed by reversely zoned euhedral outer rims. The reversed zoned phenocrysts represent a minor

249 fraction of the total orthopyroxene population and are not observed in every thin section. Some crystals  
250 have rounded cores with clinopyroxene overgrowths. The reverse zoning is interpreted to occur as a result  
251 of heating, with the clinopyroxene overgrowth rims indicating direct contact with mafic melt.  
252 Clinopyroxene normally occurs in the andesite as microphenocrysts and microlites as well as overgrowths  
253 on orthopyroxene, quartz and sometimes in the thermal breakdown rims of amphibole (Table 3); it can be  
254 very common in the groundmass of some thin sections. Clinopyroxene is also common in mafic enclaves,  
255 as microlites and microphenocrysts.

256  
257 There are three orthopyroxene phenocryst types, identified on the basis of having unzoned rims, reversely  
258 zoned rims or clinopyroxene overgrowths, all have similar core compositions (En<sub>56-70</sub>, Fs<sub>26-41</sub>, Mg# 63-  
259 68) where (Mg# = atomic units Mg/(Mg+Fe<sup>2+</sup>)). Type 1 consists of unzoned or weak normally zoned  
260 crystals with rim compositions En<sub>57-61</sub> and Wo<sub>1.8-2.3</sub>. Type 2 consists of reversed zoned crystals with rim  
261 compositions En<sub>62-73</sub> and Wo<sub>2.2-3.7</sub>. Type 3 consists of crystals with clinopyroxene overgrowths.

262 Orthopyroxene microlites have Mg#s in the range 58-74 and display the second most magnesium rich  
263 compositions of the orthopyroxenes present in the andesite after the reversed zoned phenocryst rims  
264 (Table 6a & 6b). Orthopyroxene in the mafic enclaves have similar Mg#s to the andesite microlites. The  
265 clinopyroxenes have Mg#s in the range 66-74, and they are not in equilibrium with the orthopyroxene  
266 phenocrysts of the andesite.

267

### 268 *Fe-Ti Oxides*

269 In the andesite, phenocrysts are rare while microphenocrysts (>100 μm) are common and can be zoned  
270 (Table 3) with rounded irregular cores, resorbed rims and exsolved textures. Fe-Ti oxides also occur as  
271 inclusions in the phenocrysts and microphenocrysts of amphibole, pyroxene and plagioclase, where they  
272 tend to be subhedral. Enclave microphenocrysts can be euhedral homogeneous crystals or heterogeneous  
273 crystals with exsolution textures (Table 3).

274

275 Titanomagnetite is the most common oxide in the eruptive products, with minor ilmenite present.  
276 Individual hand specimen samples can show significant inter-crystal compositional variation; the extent  
277 of the variation can be such that Devine et al. (1998a) reported observing reversed zoning in half of the  
278 titanomagnetite crystals analyzed. The oxide compositions have shown little temporal variation for the  
279 first three eruption phases. The andesite titanomagnetite microlites and enclave titanomagnetites generally  
280 have higher titanium contents than the andesite microphenocrysts with the microphenocryst rims being  
281 slightly more titanium rich than the cores.

282

### 283 *Bulk Rock Composition*

284 To date only the Phase I bulk chemistry has been published, the products are predominantly andesite  
285 displaying SiO<sub>2</sub> contents in the range (58-62 wt%), (Murphy et al., 2000; Zellmer et al., 2003a; Barclay et  
286 al., 2010), with an average composition of 59.7 wt% SiO<sub>2</sub> (Murphy et al., 2000). The enclaves are  
287 reported to have SiO<sub>2</sub> contents of 51-56 wt% (Murphy et al., 2000) and 49-55.5 wt% (Zellmer et al.,  
288 2003a). Both compositions are low-K with the andesites having a calc-alkaline affinity while the enclaves  
289 are of tholeiitic affinity (Murphy et al., 2000). Bulk geochemical trends are similar in both lava types.  
290 With increasing SiO<sub>2</sub>, TiO<sub>2</sub>, Al<sub>2</sub>O<sub>3</sub>, FeO, MgO and CaO all show decreasing trends, while Na<sub>2</sub>O and K<sub>2</sub>O  
291 show increasing trends. The Phase I andesites have relatively restricted major element compositions and  
292 the differences in the modal proportions of mineral phases were proposed as a likely source of the  
293 andesite heterogeneity within Phase I (Zellmer et al., 2003a).

294

### 295 *Initial Conclusions*

296 The experiments of Barclay et al. (1998) showed that the andesites were stored at a minimum pressure of  
297 115-130 MPa at temperatures (820-840) °C before being erupted, with measured water contents in the  
298 range (4.27 ±0.54) wt% H<sub>2</sub>O (Barclay et al., 1998), 4.7 wt% (Devine et al., 1998a) or up to 6.2 wt% H<sub>2</sub>O  
299 (Humphreys et al., 2009b). Textural characteristics of the amphibole phenocrysts such as coarser grain

300 reaction rims dominated by clinopyroxene are thought to represent thermal breakdown during reheating  
301 events, while partial to complete opacitisation, particularly along cleavage and cracks or adjacent to  
302 vesicles is thought to develop during shallow dome storage with passive gas fluxing (e.g. Garcia &  
303 Jacobson, 1979; Devine et al., 1998b; Humphreys et al., 2009b).

304

305 Couch et al. (2003b) proposed that the textural variations observed in the andesitic groundmass can be  
306 attributed to variations in ascent rates in a system undergoing open system degassing. The presence of  
307 enclaves in the erupted lavas (Murphy et al., 1998), the reverse zoning in the orthopyroxene and  
308 plagioclase phenocrysts (Murphy et al., 1998; 2000) along with the higher temperature groundmass  
309 assemblage (Humphreys et al., 2009a) were used as evidence that the eruption was triggered by an  
310 intruding mafic magma, heating and remobilizing the andesite. It was also demonstrated that amphibole  
311 fractionation is important in driving the enclave compositions (Zellmer et al., 2003a).

312

313 Reheated textures are fairly localized in the andesite (Murphy et al., 1998; 2000), which is evident in  
314 the low modal abundance of reversed zoned plagioclase and orthopyroxene phenocrysts. Based on the  
315 absence of amphibole microlites in the Phase I andesite, Murphy et al. (1998) had initially suggested that  
316 enclave disaggregation was minor if at all present. More recently, Humphreys et al. (2009a) have shown  
317 that the physical destruction and dispersion of some enclaves also contributes to the mafic nature of the  
318 microlite assemblage in the Phase II and Phase III andesite groundmass, while Genareau & Clarke (2010)  
319 showed that basaltic melt microscopically intrudes the margins of the andesite. Based on the thickness of  
320 amphibole thermal breakdown rims, extrusion occurs after reheating on time scales of hours to months  
321 (Devine et al., 2003; Rutherford & Devine, 2003; Devine & Rutherford, this volume).

322

323 Zellmer et al. (2003a) showed that the currently erupting Soufrière Hills andesite can be generated by  
324 fractional crystallization of plagioclase and amphibole from the South Soufrière Hills (SSH) basalts. In  
325 contrast, while the SSH lavas are compositionally similar to the mafic enclaves of the current Soufrière

326 Hills eruption (Figures 9 & 10), incompatible trace element ratios demonstrate that neither the current  
327 andesite nor the SSH lavas can be derived from the mafic enclaves (Zellmer et al., 2003a).

## 328 **RESULTS**

### 329 *Phases IV and V*

330 The textures of andesite samples erupted in Phases IV and V vary from the banded pumice produced  
331 during the July 28<sup>th</sup> 2008 explosion to the dome rock produced throughout both phases. We have already  
332 discussed how the volcanic activity of Phases IV and V differed to the first three extrusion phases; we  
333 now present the results of petrological and geochemical analysis from Phases IV and V.

334

### 335 *Textures*

336 The mineral phases present in the respective andesite and enclave lavas have remained consistent  
337 throughout the five eruption phases. Mineral textures associated with disequilibrium in Phases I, II and III  
338 andesites e.g. reversely zoned orthopyroxene phenocrysts, sieve textured plagioclase and embayed quartz  
339 are all observed in the andesites of Phases IV and V. Similarly to Phases I, II and III, amphibole is absent  
340 from the andesite microlite assemblage. Dome samples from Phases IV and V are generally crystal rich  
341 (~30-46% porphyritic) with phenocrysts and microphenocrysts of plagioclase, amphibole and  
342 orthopyroxene present along with microphenocrysts of clinopyroxene and Fe-Ti oxides (Figure 2). The  
343 groundmass in dome samples can be coarsely crystalline and vesicular (up to 35%) with microlites and  
344 glass present.

345

346 The enclave textures observed in Phases IV and V are also similar to those observed in the previous three  
347 phases. Plail et al. (this volume) categorizes the enclaves using parameters such as the volume of crystals  
348 inherited from the host andesite. They have identified three distinct enclave textures: a diktytaxitic  
349 framework dominated by plagioclase and pargasitic amphibole (Figure 3a); a diktytaxitic framework  
350 dominated by plagioclase and clinopyroxene (Figure 3b) and a composite (mixed enclave) of the above

351 two textures (Figure 3c). Xenocrysts (plagioclase, hornblende and orthopyroxene) are present in all  
352 enclave types (Plail et al., this volume).  
353 The inter-phase differences between andesites of the eruption may be subtle. For example, some of the  
354 dome rock samples from Phases IV and V tend to be less dense and friable; their groundmass tends to be  
355 finer grained than the denser dome blocks. The feature seems more common in Phases IV and V relative  
356 to the earlier phases. Secondly, while the mafic enclaves are ubiquitous throughout the eruption, there is  
357 an apparent increase in enclave abundance over time (see discussion in Plail et al, this volume). The  
358 average macroscopic modal abundance of enclaves in the andesite products ranges from 1-2% in the  
359 Phase I products (Murphy et al., 1998; 2000) to up to 8% in the products of Phase III (Barclay et al.,  
360 2010) and 8.5 % in Phase V (Plail et al., this volume), while Komorowski et al. (2010) report a mafic  
361 content of 12% in the tephra generated from explosions during Phase IV activity (although these three  
362 sets of values were determined using different methods).

363

#### 364 *Banded Pumice*

365 The banded sample from the July 28<sup>th</sup> 2008 explosion (sample number MVO1532d) is atypical of  
366 previously erupted samples. The sample shows clear textural heterogeneity in the form of whitish and  
367 dark grey streaks dissimilar to the chilled margins displayed by the mafic inclusions and resembles  
368 banded pumice. The sample comprises of a silicic part with pale brown to colourless glass, very few  
369 microlites and relatively low vesicularity, as well as a more mafic part which is dark brown with a  
370 crystalline groundmass and no obvious clear glass. Clearly mixed patches containing brownish glass are  
371 evident. The 'mixed' and mafic parts occur together spatially in patches hundreds of  $\mu\text{m}$  across, while the  
372 silicic parts form larger patches.

373

374 The mixed and mafic parts contain the typical assemblage present in the andesite such as phenocrysts of  
375 plagioclase with oscillatory and sieve textures, hornblendes, orthopyroxenes with clear rims or overgrown  
376 by clinopyroxene, and microlites of plagioclase + 2 pyroxenes + magnetite. In contrast, the silicic part

377 contains hornblende, no sieved plagioclase, only pristine orthopyroxene and few small microlites (~5-10  
378  $\mu\text{m}$ ) of plagioclase, orthopyroxene and titanomagnetite; clinopyroxene is absent. Hornblende phenocrysts  
379 are commonly either pristine or have a very thin incipient reaction rims (5-8  $\mu\text{m}$ ). The silicic matrix also  
380 contains numerous larger (50-200  $\mu\text{m}$ ) broken fragments of plagioclase phenocrysts. Euhedral, prismatic  
381 quartz microlites are common; these are normally ~50  $\mu\text{m}$  ( $\pm 20$ ) in size and are not typical of the  
382 Soufrière Hills andesite. They do not replace the typical rounded, embayed quartz phenocrysts, which are  
383 present as usual.

384

### 385 *Plagioclase Composition*

386 The Phase IV and Phase V andesite plagioclase phenocryst cores and rims exhibit a wide range of  
387 compositions ( $\text{An}_{46}$  to  $>\text{An}_{80}$ , Table 4) which overlaps with phenocryst compositions from the previous  
388 phases (Figure 1a). The oscillatory plagioclase cores are generally more calcic than the cores of  
389 phenocrysts with other textures (Figure 1d). The mean An content for both Phase IV and Phase V  
390 phenocryst rims is ~  $\text{An}_{56}$ , within error of the mean An contents from phenocryst rims of the previous  
391 phases (Table 4, Figure 1a). As with the first three extrusion phases, the microlite rims of Phases IV and  
392 V are more calcic than their respective phenocryst rims (Figure 1a & b, Table 4), and the enclave  
393 microlites are generally more calcic than the andesite microlites (Figure 1b). There is inter-phase  
394 variation of Fe contents in the andesite hosted microlite crystals, it is however non-systematic.

395

### 396 *Amphibole Composition*

397 Phase IV and Phase V andesite amphiboles are predominantly magnesio-hornblende, the same as the  
398 andesite amphiboles from Phases I to III (Figure 4a) with minor amounts of tschermakite. Mg-numbers  
399 are in the range 0.44-0.55. There is a systematic change in enclave amphibole FeO content (Figure 4d)  
400 from Phases I to III (unfortunately, no data from Phase IV enclave amphibole is available since no  
401 enclave products from Phase IV were collected). The enclave amphiboles from Phases I to III display a



402 steady increase in magnesium numbers (0.5 to 0.59), and the SiO<sub>2</sub> content also decreases from Phases I to  
403 III (Table 5b, Figure 4c &d). The absence of Phase IV enclave amphibole data produces an undesired gap  
404 in the dataset however, it can be seen that the Phase V enclave amphibole have higher mean contents of  
405 wt% Al<sub>2</sub>O<sub>3</sub>, MgO, CaO, TiO<sub>2</sub> and Na<sub>2</sub>O relative to the amphibole in the enclaves of the first three  
406 eruption phases (Table 5b). Apart from having the highest FeO and SiO<sub>2</sub> contents, the Phase I enclave  
407 amphiboles are lowest in wt% Al<sub>2</sub>O<sub>3</sub>, MgO and TiO<sub>2</sub>.

408

#### 409 *Orthopyroxene Composition*

410 Andesite orthopyroxene phenocryst core compositions have been relatively homogeneous throughout the  
411 eruption (En<sub>56-70</sub>, Fs<sub>26-41</sub>) with a mean magnesium number of 0.6 (Table 6a). The normally zoned rims  
412 (Mg# 0.58-0.65 mean ~ 0.61) and reversed zoned rims (Mg# 0.68-0.75 mean ~ 0.7) have been fairly  
413 unchanged during the eruption (Figure 5a). The andesite microlites generally have higher magnesium  
414 numbers, as well as higher CaO and Al<sub>2</sub>O<sub>3</sub> contents, than the phenocryst cores throughout the eruption  
415 (Figure 5b). Microlites from Phases I, II, III and IV have the same mean magnesium number of 0.67  
416 (Figure 5b). However, the microlites of Phase V have a slightly lower mean magnesium number of 0.63  
417 (Table 6a, Figure 5b).

418

#### 419 *Clinopyroxene Composition*

420 The clinopyroxene composition has varied little throughout the eruption; they are mostly augites, calcic-  
421 augites and diopsides with cores and rims in the compositional range En<sub>39-49</sub>, Wo<sub>31-47</sub> and mean  
422 compositions of En<sub>42-44</sub>, Wo<sub>40-43</sub>. Kushiro (1960) has demonstrated that it is the SiO<sub>2</sub> wt% content of a  
423 magma and not temperature that is the major control of the SiO<sub>2</sub>/Al<sub>2</sub>O<sub>3</sub> ratio of the crystallizing  
424 clinopyroxenes and that the ratio increases with increasing magma SiO<sub>2</sub> content. The andesite  
425 clinopyroxenes show distinct SiO<sub>2</sub>/Al<sub>2</sub>O<sub>3</sub> ratios by eruption phase (Table 6c). The enclave clinopyroxenes  
426 also show a similar inter-phase trend in FeO from Phase I to III like the enclave amphiboles.

427

428

429 *Oxide Composition*

430 As was the case in the first three eruptive phases, titanomagnetite is the most common oxide in the  
431 products of Phases IV and V with only minor ilmenite present. The andesite microphenocryst  
432 titanomagnetite cores and rims from the five extrusion phases have overlapping compositions (21-30  
433 mol% Usp), with no systematic variation between phases. The Phase IV microlites have higher TiO<sub>2</sub>  
434 contents (up to 16 wt%) than the microphenocrysts (7-10 wt%), as is the case with the titanomagnetites  
435 from Phases I, II and III. However, this is not the case for Phase V where the microlites have similar TiO<sub>2</sub>  
436 wt% contents to the microphenocrysts from Phase V (Table 7a).

437

438 *Glass composition*

439 The andesite and enclave glass compositions for the products of Phases IV and V have shown little  
440 variation relative to the previous phases, glass compositions have been consistently rhyolitic in both  
441 magma types (70-82 wt% SiO<sub>2</sub>) throughout the eruption (Table 8). Some authors have shown that the  
442 glass present in both magma types are essentially indistinguishable (e.g. Murphy et al., 1998; 2000),  
443 while others (e.g. Humphreys et al., 2010) have shown evidence indicating subtle differences between  
444 enclave and andesite glass. The K<sub>2</sub>O content shows a bimodal distribution of high and low K<sub>2</sub>O glass  
445 samples with some intermediate compositions observed (Figure 6).

446

447 Humphreys et al. (2010) interpreted the glass compositions enriched only in K<sub>2</sub>O, as an indication of  
448 diffusive contamination by high-K mafic inclusion glass; some samples are also enriched in TiO<sub>2</sub>,  
449 suggesting physical mixing of remnant glass. In general with increasing SiO<sub>2</sub>, there is a decreasing trend  
450 of Al<sub>2</sub>O<sub>3</sub>, while K<sub>2</sub>O increases (Figure 6). There are a few samples with SiO<sub>2</sub> contents of 80-82 wt% that  
451 have high Na<sub>2</sub>O, high CaO, low FeO and low K<sub>2</sub>O, which are likely due to post extrusion phase

452 separation of two types of glasses of differing chemistry as described by Cashman (1992) for the Mt St  
453 Helens lava dome and indicated by Humphreys et al. (2009a) for the products of Phases II and III.

454

#### 455 *Bulk Rock Composition*

456 The andesites of Phases IV and V have a similar range in bulk rock SiO<sub>2</sub> (56-62 wt%) to the products of  
457 the previous phases (Table 9). The trends of decreasing TiO<sub>2</sub>, Al<sub>2</sub>O<sub>3</sub>, FeO, MgO and CaO and increasing  
458 Na<sub>2</sub>O and K<sub>2</sub>O with evolution reported for the Phase I products are present in the products of the later  
459 eruptive phases (Figure 7). There is considerable inter-phase compositional overlap for most elements at  
460 similar SiO<sub>2</sub> contents. As is the case with the andesite, the enclave products of the later phases show  
461 compositional overlap and similar trends to the Phase I enclave products.

462

#### 463 *Whole Eruption*

##### 464 *Trends and Variations in Bulk Rock Composition*

465 There are some clear differences between the eruption phases in terms of bulk rock composition. Firstly,  
466 the FeO contents show systematic inter-phase variation with the mean FeO contents showing a clear  
467 decrease during the first three phases. The andesite products of Phase I have a mean FeO content of (7.32  
468 wt%), while the Phase II and Phase III products have mean values of 7.14 and 6.6 wt% FeO respectively  
469 (Table 9). There is a relative increase in mean FeO to 7.4 wt%, for samples erupted during Phase IV  
470 followed by a subsequent decrease in Phase V to 7.08 wt% FeO (Figure 8a, Table 9). Although not as  
471 systematic as FeO, MgO contents also show some variation in the andesite (Table 9).

472

473 The enclave bulk rock FeO trend behaves in a similar way to the andesite bulk FeO trend (Figure 8a).

474 The inter-phase contrast in FeO content is however more pronounced in the enclaves than in the  
475 andesites, thus at approximately 50 wt% SiO<sub>2</sub> there is a bulk rock compositional difference of up to 2  
476 wt% FeO between the enclave products of Phases I and III (Figure 7). One observation of note is that the  
477 difference between the mean bulk enclave FeO content and their syn-eruptive host andesites shows a

478 steady decrease with a change of ~ 1% over the eruption, from 2.3 wt% in Phase I to 1.4 wt% in Phase  
479 V, this is outside the error of the FeO contents. In other words, the difference between enclave and host  
480 FeO contents has been narrowing with time. There are also subtle differences in MgO and CaO that are  
481 outside analytical error.

482

483 Also of note is that the Phase I and Phase II andesite compositions are more scattered than those of Phases  
484 III, IV and V (Figures 7 & 10). This results in better defined linear trends of (for example) Al<sub>2</sub>O<sub>3</sub>, CaO,  
485 TiO<sub>2</sub> and Sc with increasing FeO/MgO for the andesite products from Phases III, IV and V; linear trends  
486 are also present in the enclave products of Phases III and V (Figure 10). There is a bit of scatter at higher  
487 ratios (>2.2 FeO/MgO) in the Phase III and Phase V enclaves in all of the plots. The enclave products of  
488 Phases III and V define a different slope to the Phase I and Phase II products on the SiO<sub>2</sub> vs. FeO plot  
489 (Figure 7) and thus together seem distinct from the products of Phases I and II. Phase IV enclave data are  
490 not available, but given the behaviour of the Phase IV andesite products and the apparently coupled FeO  
491 variation of both magmas, we anticipate that the bulk chemistry of the Phase IV enclaves would quite  
492 likely show well defined trends with little scatter similar to that observed in the enclaves of Phases III and  
493 V. It must be noted that the inter-phase variation in plagioclase microlite FeO content (Figure 8d) does  
494 not mirror bulk rock inter-phase FeO variation (Figure 8a).

495

496 Generally, the Phase V andesites have the highest SiO<sub>2</sub> contents while the Phase II and Phase IV andesites  
497 have the lowest SiO<sub>2</sub> contents. The Phase V enclaves are also the most SiO<sub>2</sub>-rich (Plail et al., this  
498 volume); regardless to this the SiO<sub>2</sub> contents of the enclaves and host andesites are not coupled. This is  
499 highlighted by the Phase II enclaves being more SiO<sub>2</sub>-rich than the Phase I and Phase III enclaves (Table  
500 9). The Phase V andesites also show elevated total alkali contents, relative to Phases I, III and IV  
501 andesites (Figure 5c) as well as lower wt% TiO<sub>2</sub>, Al<sub>2</sub>O<sub>3</sub>, MgO and CaO (Table 9). Phase IV andesites  
502 have the highest wt% FeO, MgO and Al<sub>2</sub>O<sub>3</sub> while the Phase II andesites are richer in CaO wt%. The  
503 Phase V enclaves are richer in total alkalis.

504

505 Due to its amalgamated nature, the integrity of the bulk rock data set needs be examined in order to verify  
506 whether the observed variations in FeO are real or an artifact of using different laboratories over several  
507 years. This is addressed in Appendix I where we show that the observed variations are independent of  
508 laboratory bias and are indeed real.

509

### 510 *Estimates of temperature, pressure, water content and log fO<sub>2</sub>*

511 A number of different methods have been used to estimate the pre eruption temperatures of the andesites  
512 and mafic enclaves, including estimates obtained from orthopyroxene (using QUILF, Anderson et al.,  
513 1993) in single pyroxene mode, following Murphy et al. (2000), use of magnetite-ilmenite pairs (e.g.  
514 Devine et al., 2003), the hornblende-plagioclase geothermometer of (Blundy & Holland, 1990), the 2-  
515 pyroxene geothermometer of Lindsley (1983), the plagioclase-liquid thermometer of (Putirka, 2005), and  
516 clinopyroxene-melt equilibria of Armienti et al. (2007), after Putirka et al. (1996; 2003) and Putirka  
517 (1999) which also produces pressure estimates. Pressures were also estimated with VolatileCalc  
518 (Newman & Lowenstern, 2002) by measuring glass volatile contents and assuming H<sub>2</sub>O saturation.

519

520 For Phase I, these approaches generated values of 785-980 °C for the andesite orthopyroxene phenocryst  
521 cores with an average of 851 ±20 °C (Murphy et al., 1998; 2000), a similar temperature range of 834-850  
522 °C was obtained by Devine et al. (1998a), and 820-840 °C by Devine et al. (2003) both using magnetite-  
523 ilmenite phenocryst pairs. This is consistent with the experiments of Barclay et al. (1998) which showed  
524 that the andesites were stored at temperatures 820-840 °C before being erupted. The reversed zoned  
525 orthopyroxene rims give higher temperatures up to 1100 °C (Murphy et al., 1998; 2000). Enclave hosted  
526 orthopyroxene cores give temperatures in the range 1020-1050 °C (Murphy et al., 1998). New data  
527 obtained by MVO for Phases II,III,IV and V (some Phase II and Phase III data reported in Humphreys et  
528 al., 2009a) are reported below and presented in Table 11.

529

530 *Pyroxene*: Orthopyroxene phenocryst cores in the andesite give temperatures of 824-965 °C (mean 866  
531 °C), with unzoned rims at 845-895 °C (mean 869 °C) and reversely zoned rims at 1018-1032 °C (mean  
532 1025 °C). Orthopyroxene inclusions in other minerals or in crystal clots also gave low temperatures 791-  
533 809 °C. Orthopyroxene microlites in the andesite gave temperatures of 958-1017 °C, while orthopyroxene  
534 in mafic enclaves gave 903-1305 °C (mean 1070 °C), with 1074-1196 °C for the two-pyroxene  
535 geothermometer. These two-pyroxene temperatures may not reflect equilibrium conditions.

536 *Plagioclase-liquid*: the plagioclase-liquid thermometer produced a wide range of temperatures from 821  
537 °C (for melt inclusions trapped in plagioclase phenocrysts) to 1100 °C (for matrix glasses paired with  
538 microlite rims); with increasing temperatures correlating with decreasing melt H<sub>2</sub>O content. This is  
539 similar to the style of variation reported in Blundy et al. (2006) but given the huge range in temperature  
540 we suggest that many of the higher groundmass temperatures may reflect disequilibrium.

541

542 *Hornblende-plagioclase*: Inclusions of plagioclase in andesite hornblende phenocrysts give temperatures  
543 in the range 804-890 °C (mean 833 °C). Paired analyses from crystal clusters, interpreted as fragments of  
544 disaggregated mafic enclaves, give temperatures of 849-947 °C (mean 894 °C).

545

546 *Clinopyroxene-melt*: The clinopyroxene-melt thermometer gave temperatures in the range 1097-1145 °C  
547 (mean 1110 °C) for microlites/matrix glass and microphenocrysts/matrix glass in the mafic enclaves. As  
548 with the two-pyroxene and plagioclase-melt temperatures, these may not reflect equilibrium conditions.

549

550 *Pressure and water estimates*: Pressure estimates obtained from the Cpx-melt equilibrium for crystals  
551 from both enclaves and andesite range from 10-280 MPa with a mode of 50-100 MPa. Previous  
552 measurements of melt H<sub>2</sub>O contents from melt inclusions are in the range 4.27 ± 0.54 wt% H<sub>2</sub>O (Barclay  
553 et al., 1998), ~4.7 wt% (Devine et al., 1998a) and 1.1-6.2 wt% (Humphreys et al., 2009b). Assuming  
554 water saturation in the absence of CO<sub>2</sub> (Newman & Lowenstern, 2002), these estimates equate to  
555 pressures up to 214 MPa which is consistent with the estimates from the Cpx-melt equilibrium.

556 *Temperature variation*

557 Different methods tend to produce distinct temperature ranges and this is probably because they are  
558 recording temperatures from different parts of the reservoir or localized equilibrium at differing times.  
559 Taken together, the hb-plag temperatures, single-orthopyroxene core temperatures, 2-oxide temperatures  
560 and plagioclase-liquid temperatures from melt inclusions are probably representative of phenocryst  
561 crystallization and hence the ambient temperature within the andesite storage region. These temperatures  
562 are typically in the range 785-900 °C with an average at the lower end of that range and are consistent  
563 with the experiments of Barclay et al. (1998) on Phase I products.

564  
565 Higher temperature estimates are obtained from the disequilibrium features outlined above, e.g. 826-1101  
566 °C from reverse zoned orthopyroxene rims (Table 11). This is consistent with the very An-rich  
567 compositions observed in sieved plagioclase crystals, which requires very high temperatures and a more  
568 mafic melt (Couch et al., 2003a). These temperatures are inferred to be recording the reheating of the  
569 andesite crystals by the basalt intruding into the base of the reservoir. The estimates from the enclaves are  
570 expectedly higher, 903-1305 °C for the single orthopyroxene method, 1074-1196 °C using the 2 pyroxene  
571 method and 1097-1145 °C using the clinopyroxene-melt equilibrium, although some of these  
572 temperatures may also reflect disequilibrium mineral compositions.

573  
574 The variability within these estimates may be due to heterogeneities within the andesite storage region,  
575 and/or due to the localized nature of the basaltic intrusion and thus equilibrium at higher temperatures  
576 (e.g. Pichavant et al., 2007). The temperature estimates obtained using the various methods all show a  
577 range of values with the smallest difference between maximum and minimum temperatures being 14°C  
578 for any given method. There is no evidence in our data to suggest systematic changes in temperature as  
579 the eruption proceeds. However Devine & Rutherford (this volume) used oxide thermometry to show that  
580 the mean ambient temperature of the andesite before being reheated shows a 10 °C increase from Phase I  
581 (825 °C) to Phase V (835 °C).

582 *Estimates of log fO<sub>2</sub>*

583 Log *f*O<sub>2</sub> values calculated from andesite hosted ilmenite-magnetite pairs are presented in Table 8. The  
584 inter-phase values show some overlap with no clear trend. The Mg-Fe exchange coefficient K<sub>d</sub>, (Putirka  
585 et al., 2003) is used to establish mineral melt equilibrium of clinopyroxenes where  $K_d \text{ cpx-liq} = [(X \text{ MgO}$   
586  $\text{liq} / X \text{ FeO Cpx}) / (X \text{ MgO Cpx} / X \text{ FeO liq})]$ . Suitable mineral-melt equilibrium is thought to be attained  
587 when a K<sub>d</sub> value of 0.27±0.03 is obtained for clinopyroxene. Bédard (2010) showed that clinopyroxene  
588 K<sub>d</sub> values will vary as a function of temperature, pressure, log *f*O<sub>2</sub> as well as melt SiO<sub>2</sub> and, total alkalis.  
589 Box plots of clinopyroxene microlite K<sub>d</sub> values by eruption phase are presented in Figure 5d, the K<sub>d</sub>  
590 value for the clinopyroxene microlites varies by eruption phase with Phase III having the highest median  
591 values while Phases V and II have the lowest median values. The data obtained from the Cpx-melt  
592 equilibria showed no systematic variation in pressure and temperature with eruption phase. The total  
593 alkali contents display a negative correlation with the clinopyroxene K<sub>d</sub> values, hence it seems the Cpx  
594 K<sub>d</sub> values are responding to changes in total alkali content and not log *f*O<sub>2</sub>.

595

## 596 **DISCUSSION**

597 Although the andesitic rocks erupted since 1995 at Soufrière Hills are fundamentally similar in terms of  
598 textures and mineral compositions, there are some key systematic variations over time that may reveal  
599 details about the nature of the plumbing system at depth. In particular, the key observation is that the bulk  
600 rock FeO content of both andesite and enclave appear to be coupled. Both andesites and enclaves from  
601 Phases I and II show higher major element oxide contents apart from SiO<sub>2</sub>, and more scatter at similar  
602 FeO/MgO ratios compared with the later phases (Figure 10), they also have higher CaO/Al<sub>2</sub>O<sub>3</sub> ratios at  
603 similar FeO/MgO ratios. Here we review the overall relationships between the andesite and enclave  
604 magmas and hence interpret the possible causes of these compositional variations.

605



606 Mt Pelée Martinique has produced a spectrum of products ranging from basaltic-andesites to dacites;  
607 some compositions were only erupted at certain periods in the volcano's history due to the changing  
608 nature of volcano's plumbing system with time (Fichaut et al., 1989a). Andesites are however ubiquitous  
609 in the Mt Pelée deposits and have been of a similar composition for the past 100,000 years (Dupuy et al.,  
610 1985). The Mt Pelée andesites also contain microlites inherited from intruding basalts (Martel et al.,  
611 2006) as do the Soufrière Hills andesites (Humphreys et al., 2009a).

612 The volcanic stratigraphy and petrology of Mt Pelée, is well constrained and the physical evolution of the  
613 plumbing system through time has been modeled (Fichaut et al., 1989a). It has been established that the  
614 current shallow reservoir is zoned (Dupuy et al., 1985, Pichavant et al., 2002) and is relatively small (<  
615 1km<sup>3</sup>) at about 10km bsl (Fichaut et al., 1989a). It has also been established that the basaltic magmas are  
616 parental to the andesites via magma mixing and fractional crystallization (Fichaut et al., 1989b).

617

618 Magma mixing occurs in relation to basaltic intrusions which generate eruptions with heterogeneous  
619 magma compositions (e.g. Fichaut et al., 1989a; Gourgaud et al., 1989), they are normally larger in  
620 volume than the homogeneous eruptions since lower parts of the reservoir gets tapped (Dupuy et al.,  
621 1985). Fractional crystallization of the hybrid magmas created by the mixing events produces fairly  
622 homogeneous magmas which tend to evolve towards more acid compositions; these are the magmas that  
623 feed the smaller volume homogeneous eruptions (Fichaut et al., 1989a; Pichavant et al., 2002). Thus  
624 andesite generation at Mt Pelée is fairly well understood.

625

#### 626 *Andesite phenocryst-groundmass relationship*

627 In the current Soufrière Hills eruption, microlite rims and some cores are generally more mafic than  
628 phenocryst rims (in the case of plagioclase) or both cores and rims (in the case of orthopyroxene). This is  
629 contrary to what is expected from closed-system crystallization and cooling, and demonstrates the effects

630 of mafic magma input and the short time scale between heating and eruption. The nature and extent of  
631 physical interaction between the andesites and basalts is also evidenced in the ubiquitous presence of  
632 mafic enclaves within the andesite, as well as rarer macroscopic features such as the banded pumice. The  
633 contrasting temperatures of the intruding mafic magma and the silicic host also leads to heat transfer  
634 (Snyder, 2000), resulting in remobilization of the andesite (Murphy et al., 2000).

635  
636 The andesite contains various disequilibrium textures which provide evidence of reheating driven by  
637 mafic magma, including reverse zoned orthopyroxene (Barclay et al., 1998; Murphy et al., 1998; 2000);  
638 sieve textures and calcic overgrowth rims on plagioclase phenocrysts (Couch et al., 2003a); two oxide  
639 disequilibrium (Devine et al., 1998a; 2003); resorbed quartz with clinopyroxene mantles; thermal  
640 breakdown of amphiboles (Humphreys et al., 2009b); and clinopyroxene overgrowths on orthopyroxene  
641 (Murphy et al., 1998; Humphreys et al., 2009a). These observations are consistent with the higher range  
642 of temperatures obtained from the andesite by some of the thermometry methods employed.

643  
644 *Other Disequilibrium Features*  
645 The andesite microlite assemblage generally consists of normally zoned plagioclase with euhedral to  
646 hopper or skeletal textures (suggesting rapid growth, Hammer & Rutherford, 2002), normally zoned  
647 orthopyroxenes, and normally zoned clinopyroxenes with a skeletal appearance. Although all  
648 orthopyroxene microlites are typically more mafic than phenocryst rims, they are not always  
649 compositionally identical to the enclave microlites, but can sometimes exhibit intermediate or even more  
650 mafic compositions relative to some enclave microlites (Figure 5b).

651  
652 The absence of groundmass amphibole in the Phase I andesite and the proposed compositional differences  
653 between the plagioclase groundmass in the Phase I andesite and the enclave plagioclase were used as  
654 evidence against enclave disaggregation being a significant process (Murphy et al., 2000), the absence of  
655 groundmass amphibole in the andesite was also used by Couch et al. (2003a) as evidence against magma

656 mixing. More recently (Humphreys et al., 2009a; Genareau & Clarke, 2010; Humphreys et al., 2010)  
657 proposed enclave disaggregation and mixing as significant processes to support chemical and textural  
658 observations in the products of Phases II, III and IV.

659  
660 We have also shown that the Phase I andesite plagioclase microlite population has elevated Fe contents  
661 similar to the enclave plagioclase and the andesite microlites from subsequent phases (Table 4, Figure  
662 1e), which suggests that disaggregation probably did occur during Phase I. We have also highlighted the  
663 dominance of normally zoned plagioclase microlites in the andesite. These additional observations  
664 suggest that the mafic signature of the Soufrière Hills andesite groundmass may not be due to a simple  
665 case of crystal transfer due to enclave disaggregation, and that reheating and recrystallization of resident  
666 crystals might also be an important process in generating the hotter groundmass assemblage. The lack of  
667 change in modal abundance of reverse zoned plagioclase and orthopyroxene phenocryst indicates that the  
668 heating is still ongoing on a scale that has remained relatively unchanged. Finally, we suggest that the  
669 dominance of normally zoned plagioclase microlites reflects decompression-driven crystallization  
670 continuing after enclave disaggregation.

671  
672 The microprobe  $\text{SiO}_2/\text{Al}_2\text{O}_3$  ratio of crystallizing clinopyroxene is heavily dependent on the bulk wt%  
673  $\text{SiO}_2$  content of the host magma (Kushiro, 1960); with increasing bulk rock  $\text{SiO}_2$  favouring increased  
674  $\text{SiO}_2/\text{Al}_2\text{O}_3$  ratios in the cpx crystals. Thus the higher  $\text{SiO}_2/\text{Al}_2\text{O}_3$  values of the Phase V microphenocrysts  
675 (Table 6c) suggests that the clinopyroxene microphenocrysts found in Phase V andesites crystallized in a  
676 more  $\text{SiO}_2$ -rich melt relative to the microphenocrysts from the first three phases. There are a number of  
677 other observations for the Phase V andesites such as the elevated total bulk rock alkali contents relative to  
678 Phases I, III and IV andesites (Figure 5c); lower  $\text{TiO}_2$  wt% contents in the oxide microlites (Table 7a) and  
679 the slightly lower magnesium numbers of the orthopyroxene microlites (0.63) (Table 6a, Figure 5b) that  
680 are all consistent with the Phase V andesite products being more evolved.

681

682 *Bulk Rock Variation*

683 *Enclave Compositions*

684 The fundamental trends in the enclaves are related to fractional crystallization. The enclave products of  
685 Phases I and II are much more scattered compositionally (Figure 10). We interpret the scatter in the Phase  
686 I and Phase II enclaves as an indication of assimilation of plutonic residues remaining from previous  
687 mafic injections. There is a bit of scatter in the more evolved samples ( $>2.2$  FeO/MgO) of the Phase III  
688 and Phase V enclaves in all of the plots; the linear trends observed in the enclave products of Phases III  
689 and V could be consistent with fractional crystallization, less affected by assimilation processes. Hence  
690 the minimal scatter in the Phase III and Phase V enclaves indicates they may have erupted through a  
691 relatively residue-free pathway.

692

693 Irrespective of the scatter present in the products of Phases I and II there are still discrepancies in  
694 compositions of the enclave products that need to be accounted for. The ratios of incompatible trace  
695 elements should not be affected by shallow crustal process therefore; incompatible trace element ratios  
696 should be representative of the source region. The near constant ratio of Zr/Rb in the mafic enclaves  
697 (Table 10) indicates a fairly homogeneous source composition and suggests that the observed major  
698 element differences are likely due to differentiation rather than heterogeneities in the source region. There  
699 are a number of possible processes that might cause the enclave compositions to change and to better  
700 constrain why, we address the following relevant questions.

701

- 702 i. Are the discrepancies purely due to the effects of contamination, thus are Phase I and Phase II  
703 enclaves more hybridized products of the same magma, parental to the products of Phases III and  
704 V?
- 705 ii. Are the enclave compositions representing localized compositions in a chemically heterogeneous  
706 basaltic system?

707     iii.    Do the enclaves of each phase represent discrete chemically distinct batches of basalt magma  
708            from depth?

709

710    *Assimilation of plutonic residue*

711    Earthquake swarms in the century leading up to the current eruption were considered to represent the  
712    intrusion of basalt into the andesite storage area (Shepherd et al., 1971). The mafic magma interacting  
713    with the andesite will over time cool and crystallize, resulting in crystals accumulating at the base of the  
714    reservoir. Subsequent intrusions of basalt may therefore interact with any crystal mush or plutonic residue  
715    present, assimilating crystals and creating hybridized liquid compositions. Thus it is possible that the  
716    primary magma composition intruding into the andesite reservoir has not changed with time, but the  
717    compositions of the early erupted products of Phases I and II are driven by contamination from residue  
718    left from previous basaltic intrusions into the andesite reservoir. If this were the case, then the bulk  
719    chemistry for enclave products from Phases III and V should be generally more basic than the products of  
720    Phases I and II, and the bulk enclave compositions of the Phases I and II should be reproducible by  
721    addition of crystals to the bulk enclave compositions of Phases III and V.

722

723    There are a number of observations inconsistent with this model. First is that most recent enclave  
724    products of Phase V are more evolved than the earlier enclave products (Plail et al this volume).  
725    Secondly, crystal accumulation would increase the SiO<sub>2</sub> contents of the Phase I and Phase II enclave  
726    products and drive them towards the compositions of the Phase III and Phase V enclave products on the  
727    SiO<sub>2</sub> vs. FeO/MgO plot (Figure 10). Thus there is therefore no evidence to suggest that the enclave  
728    compositions of Phases III and V represent less hybridized liquids of the same magma batch that  
729    produced the enclaves of Phases I and II and we therefore reject this theory. This however indicates that  
730    there are other processes influencing the enclave compositions other than simple crystal assimilation and  
731    fractional crystallization.

732

733 *Stratified reservoir*

734 Chemical heterogeneity within a magma reservoir could be characterized by vertical compositional  
735 stratification due to the relationships between magma density and chemistry, with the less evolved, denser  
736 magmas residing in the lower regions of the reservoir (e.g. Trail and Spera, 1990), as is the case in the  
737 present day reservoir of Mt Pelée (e.g. Dupuy et al., 1985, Pichavant et al., 2002). Continuous or periodic  
738 tapping of a vertically heterogeneous reservoir is thus expected to produce a compositional variation  
739 towards lesser evolved lavas as the deeper reservoir is tapped, but this is inconsistent with the more  
740 evolved nature of the Phase V enclaves (Plail et al. this volume); therefore we do not accept this model for  
741 explaining the inter-phase enclave and andesite compositional variations.

742

743 *Distinct chemical pulses*

744 The nickel contents of the enclaves are all <20 ppm and they are hence not representative of primary  
745 compositions, which would be expected to have 200-300 ppm nickel (Rhodes & Dungan, 1977). The  
746 absence of modal olivine and the presence of modal plagioclase are also consistent with the parental  
747 compositions of the enclaves not being primary. Therefore the magma injected into the base of the  
748 andesite reservoir must have previously undergone differentiation, most recently in the deeper reservoir of  
749 the Soufrière Hills magma system at 10-13km (e.g. Elsworth et al., 2008; Foroozan et al., 2010; 2011).  
750 This is consistent with the fractional crystallization trends present in the Phase III and Phase V enclaves.  
751 However, the nature of basalt delivery into the base of the Soufrière Hills andesite reservoir is still a  
752 matter of discussion. A scenario of continuous recharge is proposed by Wadge et al. (2010) and Foroozan  
753 et al. (2011) due to the patterns observed in the GPS deformation signal. Contrary to this, Humphreys et  
754 al. (2009b) showed that the amphibole phenocrysts in the andesites have variations in their molar (Cl/OH)  
755 ratios and temperatures attributed to non-continuous volatile release which likely coincide with basalt  
756 recharge episodes.

757

758 If the basalt input into the base of the andesite reservoir is pulsed, then the enclaves from each eruption  
759 phase may represent chemically distinct magma pulses entering the andesite reservoir. The liquids likely  
760 represent melts from the same reservoir whose compositions are being driven by differentiation processes  
761 occurring on timescales shorter than that of the eruption. Edwards & Russell (1998) have demonstrated  
762 that AFC processes in basalts can occur on the time scale of weeks to years, a timescale which is  
763 consistent with the timescale of the first three extrusion phases and intermediate pauses. This model of  
764 periodic basalt delivery is also consistent with the observations of periodic heating Zellmer et al. (2003b),  
765 periodic volatile release Humphreys et al. (2009b) and the short time scales of hours to months between  
766 reheating, mixing and eruption of the hybrid material (e.g. Snyder, 2000; Devine et al., 2003; Humphreys  
767 et al., 2010; Devine & Rutherford, this volume ). This model is thus consistent with the petrological and  
768 geochemical data and is therefore accepted as a possible cause for the basalt compositional variation.

769

#### 770 *Enclave Amphibole*

771 We have demonstrated that the inter-phase variation of FeO content in enclave amphibole mirrors FeO  
772 variation in the bulk rock for the first three extrusion phases (Figure 4d, Figure 8a), and that there is a  
773 systematic inter-phase increase in the enclave amphibole Mg# (Figure 4c, Table 5b), and an inter-phase  
774 trend of increasing Mg and Al with falling Si from Phases I to III (Table 5b).

775

776 The composition of amphibole is heavily influenced by the composition of the liquid from which they  
777 crystallize. In particular, the Al content is related to crystallization pressure (Hammarstrom & Zen, 1986;  
778 Hollister et al., 1987; Johnson & Rutherford, 1989; Rutter et al., 1989; Blundy & Holland, 1990; Schmidt,  
779 1992; Devine et al., 1998a; Ernst & Liu, 1998; Ridolfi et al., 2010). This is consistent with the  
780 experimental data of Barclay et al. (1998) which showed that higher pressure crystallization runs on the  
781 Soufrière Hills andesite products produced amphiboles with higher Al contents than the amphiboles  
782 which occurred naturally in the lavas. Variations in amphibole Al content can also be influenced by  
783 temperature and  $fO_2$  (Bachmann & Dungan, 2002; Anderson & Smith, 1995). In general for calcic

784 amphiboles, increasing P and T leads to increases in MgO, Mg# and Al, while decreases in Si along with  
785 total (Fe + Mn + Ca) can also be expected.

786  
787 There are no independent crystallization temperature estimates for the enclave amphiboles and hence no  
788 way to assess how much influence the temperature or pressure has on the enclave amphibole Al contents.  
789 The increasing Mg#s in the enclave amphiboles from Phases I to III are consistent with the parental  
790 magmas becoming increasingly mafic from Phase I to Phase III. This would also explain the decreasing  
791 Si and increasing Al, and would be consistent with increasing crystallization temperatures. We do note  
792 however that the high Al and Ca contents coupled with high Mg#s of the Phase V enclave amphiboles  
793 (Table 5b) is inconsistent with the more evolved nature of the host magmas as indicated by Plail et al.  
794 (this volume). We also note that the lack of systematic inter-phase variation in the andesite-derived  
795 amphiboles is consistent with fairly stable crystallization conditions.

796  
797 To summarize, the pattern of varying bulk rock enclave compositions is consistent with temporal  
798 variations in the composition of the parental mafic magma entering the volcanic system at depth. This can  
799 also explain the coupled changes in enclave amphibole composition, which is consistent with  
800 crystallization from an increasingly more mafic melt for the first three extrusion phases.

801

### 802 *Andesite Compositions*

803 The observed chemical heterogeneities in the Phase I andesitic products are attributed by Murphy et al.  
804 (2000) to the proposed mode of formation, which is mainly the disaggregation and remobilization of  
805 multiple previously intruded andesitic bodies. The scatter present in the Phase I andesite is similar to that  
806 observed in the Phase I enclaves; and lessening of the scatter as the eruption proceeds is also present in  
807 the andesite as well as the enclaves. The behaviour of FeO in both lava types suggests that the  
808 composition of both is coupled to some extent, but the reason for this is not clear. We suggest that the  
809 bulk andesite compositions may be dependent on the composition of the syn-erupted basalt with which it



810 interacts, inheriting the geochemical imprint of the mafic magma. Below we consider the possible  
811 mechanisms for transferring such a geochemical signature from the mafic magma to the andesite.

812

### 813 *Andesite Hybridization*

814 Hybridization requires mass transfer which has been shown to occur at the Soufrière Hills with the  
815 proposed processes ranging from simple crystal transfer, (Murphy et al., 1998; 2000) to the physical  
816 destruction of the enclaves by varying mechanisms (e.g. Humphreys et al., 2009a; Edmonds et al., this  
817 volume; Plail et al, this volume), to localized mixing, percolation and incorporation of melt into the host  
818 andesite margins (Genareau & Clarke, 2010). It must be noted that although not systematic and coupled  
819 like FeO, inter-phase variation is still observed in all of the major elements of both lava types. The  
820 elevated Ca, Al and Mg contents of the groundmass assemblage makes it apparent that Fe is being  
821 systematically transferred from the enclaves to the host andesite while the other major elements are  
822 transferred on a more irregular basis. Therefore the process/processes responsible for transferring the Fe  
823 signature from enclave to andesite must be examined.

824

### 825 *Enclave disaggregation*

826 Variations in the FeO contents of enclave clinopyroxene and amphibole are similar to the observed bulk  
827 rock variations, while no systematic variation in FeO is observed for any of the other enclave mineral  
828 phases. We therefore suggest that a possible explanation for the bulk rock compositional variation is the  
829 physical destruction of mafic enclaves, and incorporation of clinopyroxene and amphibole crystal  
830 fragments into the andesite. The presence of high-Al amphibole fragments in the groundmass of Phase II  
831 and Phase III andesite supports such a process.

832

833 This model was tested by performing mass balance calculations on the andesite compositions using FeO  
834 content as the index for choosing end members, which are the low FeO and high FeO samples within each  
835 eruption phase. We use the enclave mineral compositions present in each respective phase for the

836 calculations. If enclave destruction is responsible for the Fe signature in the andesite then the mass  
837 balance results should be consistent with the low modal occurrence of high Al amphibole fragments in the  
838 groundmass. However, the goodness of fit (reflected by  $R^2$  values) for our modeled results is rather low,  
839 and the results show that the required mass of crystals to be added is inconsistent with the observed  
840 modes (Table 12). Therefore this model for Fe transfer is rejected.

841

#### 842 *Diffusion/advection from enclaves*

843 Grasset & Albarede (1994), propose a mechanism whereby diffusion and buoyancy-driven convection are  
844 responsible for the chemical exchange between mafic enclaves and their hosts. They propose that the  
845 density difference between the enclave and host will induce relative motion which entrains the enclave-  
846 host interface thus generating a flow pattern inside the enclave. Thermal equilibrium occurs on much  
847 shorter time scales than chemical equilibrium via diffusion (Sparks & Marshall, 1996) thus hybridization  
848 by chemical diffusion requires both magmas be liquid and the presence of mobile fluids for transporting  
849 the chemical species.

850

851 The chilled margins and abundant interstitial voids in the enclaves (Murphy et al., 1998), suggest that the  
852 enclaves were intruded into the andesite as liquid blobs (e.g. Bacon, 1986; Clyne, 1999; Saito et al.,  
853 2003). These textures however also indicate fairly rapid heat transfer and quenching, their high  
854 vesicularity suggest that they may be permeable to gas flow and melt percolation. The small size of the  
855 enclaves and short timescales (days to months) between reheating, mixing and eruption (Snyder, 2000;  
856 Devine et al., 2003; Humphreys et al., 2010) will greatly restrict the volume of andesite that could be  
857 contaminated by diffusion or advection from enclaves, and we reject this model based on time and  
858 surface area constraints.

859

860

861

862 *Diffusion/advection from basal flow*

863 Due to the difference in density between the two magmas, basaltic injections into silicic chambers may  
864 tend to occupy the base of the reservoir. Here the intricacies of the mixing could result in significant  
865 hybridization of small volumes of silicic magma, trapped beneath the intruding mafic magma (e.g. Snyder  
866 & Tait, 1995; 1998a; 1998b). Snyder & Tait (1998b) propose that isotopic and trace element signatures  
867 can be transferred from basalt to andesite without significant effect on the major element chemistry apart  
868 from FeO. This is achieved through a combination of diffusion and advection via the large surface area of  
869 the fingered morphology created by the trapped andesite rising up through the overriding basalt due to  
870 differences in density (Snyder & Tait, 1995; 1998a; Perugini & Poli, 2005).

871

872 Contamination of the andesite will increase its density due to water loss to the basalt and the migration of  
873 FeO from the basalt to the andesite. The contaminated liquid thus forms a layer between the basalt and  
874 uncontaminated andesite, in the same region where enclave formation is thought to occur (e.g.  
875 Eichelberger, 1980; Thomas et al., 1993). The relatively higher temperature of the contaminated andesite  
876 layer should delay quenching, thus giving more time for diffusion from the upper layer of the basalt.  
877 The relatively higher density of the contaminated andesite liquid should make it easier for the basaltic  
878 liquids to physically interact with and generate vesiculated blobs as enclaves into the contaminated  
879 andesite (e.g. Thomas & Tait, 1997). Both compositions are subsequently erupted together as enclaves  
880 and host andesite. Such a process would be consistent with the FeO content of the enclaves and their host  
881 andesite lavas being coupled.

882

883 For a series of injections closely spaced in time, the process is repeated and any remnant contaminated  
884 andesite liquids are further contaminated by the new influx. Subsequent basalt intrusions would create a  
885 step like dispersal of the contaminants upwards via double diffusive convection. Rather than a rapid  
886 dispersal via convection, trace element and isotopic gradients will be set up in the andesite as a function  
887 of the number of injections encountered.

888 However if each injection leads to total extrusion of the contaminated liquid, the extruded andesite should  
889 have an imprint that is only controlled by the relative chemistry and volume of the basalt it encounters.  
890 There is no robust trace element and isotopic dataset for products erupted after Phase I, so we cannot test  
891 this model conclusively. However the migration of FeO from the basalt to the andesite as predicted by the  
892 model is consistent with our observations of the coupled FeO behaviour in both magmas and this  
893 therefore seems a good way to explain the behaviour of Fe in both magmas.

894  
895 We previously highlighted a steady decrease in the gap between the Fe content of the andesite and the  
896 syn-erupted enclaves as the eruption progresses. This could be due to Fe-diffusion becoming more  
897 efficient with time. A second more plausible possibility is that residual liquids are being further  
898 contaminated over time by subsequent basalt influxes, and hence more efficient mixing may be occurring  
899 as the eruption proceeds due to the converging chemistries of the contaminated residue and the intruding  
900 basalt. We interpret the closing gap in relative bulk Fe contents as an indicator of further contamination of  
901 un-erupted previously contaminated andesite. This observation is consistent with a periodic basalt  
902 delivery into the andesite reservoir rather than a continuous trickle.

903  
904 *Gas fluxing*

905 It has been demonstrated that the intruding basalt is the primary source of the SO<sub>2</sub> that is emitted from the  
906 Soufrière Hills volcano (Edmonds et al., 2001). The volcano has exhibited a type of behaviour termed as  
907 persistent degassing (Shinohara, 2008). Thus there has been a constant influx of volatiles into the andesite  
908 reservoir from the intruding basalt. The SO<sub>2</sub> flux through the andesite reservoir varies on timescales  
909 ranging from weeks to years and in most cases is independent of magma extrusion (Christopher et al.,  
910 2010). There is no evidence to indicate that the fluxing of volatiles through the andesitic system has a  
911 major influence on the andesitic groundmass composition.

912  
913

## 914 **Expected Future Trends and Behaviour**

915 The changes in magma composition from Phase III onwards, coincide with an increase in the violence of  
916 activity during the extrusion phases. To date there is no strong evidence linking eruption style to magma  
917 composition during the eruption. However we expect subsequent extrusion phases during the present  
918 eruption to produce andesite and enclaves showing coupled Fe contents with both compositions showing  
919 similar inter-phase Fe trends. The Fe content of both magma types is further expected to converge due to  
920 the continued Fe enrichment from the repeated contamination of previously contaminated un-erupted  
921 andesite residue. We also expect the products of subsequent phases to show linear trends with little  
922 scatter.

923

## 924 **Future Research**

925 The variation in FeO content observed in the enclaves indicates significant changes in the basalt  
926 composition. It would be therefore useful to constrain the nature of basalt delivery into the andesite  
927 reservoir. Several petrogenetic processes are occurring contemporaneously during this eruption such as  
928 magma mixing, fractional crystallization, mafic recharge and possibly crustal contamination; all of which  
929 influence the magma compositions. The effects of each are poorly constrained and need to be deciphered  
930 by robust analysis of the trace element and isotopic geochemistry. The current trace element dataset is  
931 sparse and thus needs supplementing. Trace element and isotope data of the crystal cargo would also help  
932 better constrain the interaction between the basalt and andesite as well as any recharge episodes that  
933 would have occurred (e.g. Tonarini et al., 1995; Browne et al., 2006; Davi et al., 2009).

934

935

936

937

938

939 **Conclusions**

940 i. Basaltic intrusion and the subsequent formation of mafic enclaves have played an integral role in  
941 eruptions at the Soufrière Hills volcano for millennia. The intruding basalt has been providing  
942 heat to the surrounding host andesite magma and hence energy for remobilizing the andesite  
943 throughout the current eruption.

944  
945 ii. The early intruded basalt erupted in Phases I and II assimilated plutonic residue left over from  
946 previous basalt intrusions, while the basalt products of Phases III, IV and V encountered a  
947 relatively residue free reservoir floor.

948  
949 iii. There are genuine inter-phase changes in the composition of the basalt arriving from depth,  
950 especially in the FeO content.

951  
952 iv. Crystal fractionation of the basalt and subsequent mixing/mingling and diffusion produces a  
953 whole suite of hybrid magmas which are erupted as enclaves and host andesites; hence we are  
954 unable to sample the true composition of the intruded basalt or the pre intrusion andesite.

955  
956 v. The andesites are likely hybridized by the basalt due to trapping of ambient andesite liquid  
957 beneath the basal intrusion which allows for diffusion and transfer of the basalt Fe signature to  
958 the andesite while it percolates upward through then resides on the basalt sheet. Transfer of  
959 elements such as Ca, Al and Mg are controlled predominantly by mixing and enclave destruction.

960

961 **Acknowledgements**

962 MCSH is supported by a Royal Society University Research Fellowship. We acknowledge assistance  
963 from Victoria Smith and Chiara Petrone during electron microprobe analysis as well as Crystal Mann for  
964 her helpful discussion. We also acknowledge the support of the British Geological Survey.

## Appendix I - Possible inter-laboratory variability

965  
966  
967  
968  
969  
970  
971  
972  
973  
974  
975  
976  
977  
978  
979  
980  
981  
982  
983  
984  
985  
986  
987  
988

The majority of bulk rock geochemical data collected and presented here for the first three phases of extrusion are from two main labs, Brown University (Joe Devine) and University of Leicester (Murphy and Sparks, 1999; Murphy et al., 2000; Zellmer et al., 2003a; MVO contract), with additional data from the labs at Bristol University, McGill University, British Geological Survey and University of East Anglia. To rule out laboratory bias as a source of the inter-phase FeO variation, we generated plots of FeO vs. SiO<sub>2</sub> for products from Phases I, II and III (Figure 11) demarcated by data source and eruption phase.

Despite some scatter, andesite analyses from a given eruptive phase overlap within error regardless of the laboratory used. For example, Phase II andesites clearly show reduced FeO contents relative to Phase I andesites while the Phase III andesites generally have lower FeO contents than Phase II andesites at similar SiO<sub>2</sub> (Figure 11a). The same pattern is true for the mafic enclaves where the Phase III products from two different labs have distinctly lower FeO contents (Figure 11b). To further investigate this, andesite and enclave splits from Phase I products were recently analyzed at the UEA lab and are included on the plot (Figure 11a & b). They show similar FeO contents to Phase I analyses from other labs (Figure 11a & b). We are therefore confident that the variations in Fe content are real and not a function of source laboratory. In addition, the correlation of FeO contents with other geochemical variables (e.g. trace elements such as Sc, Ba and V) indicates that these distinct FeO compositions are related to real differences in bulk rock compositions and not related to laboratory analysis.

- 990 ANDERSEN D. J., LINDSLEY D. H. & DAVIDSON P.M. 1993. QUILF: A pascal program to assess equilibria  
991 among Fe-Mg-Mn-Ti oxides, pyroxenes, olivine, and quartz. *Computers & Geosciences* **19**(9), 1333-  
992 1350.
- 993
- 994 ANDERSON D.J. & SMITH D.R. 1995. The effects of temperature and  $fO_2$  on the Al-hornblende barometer.  
995 *American Mineralogist* **80**, 549-559.
- 996
- 997 ARMIENTI P., TONARINI S., INNOCENTI F. & D' ORAZIO M. 2007. Mount Etna pyroxene as a tracer of  
998 petrogenetic processes and dynamics of the feeding system. *Geological Society of America Special*  
999 *Papers*, **418**, 265-276.
- 1000
- 1001 ASPINALL W. P., MILLER A. D., LYNCH L. L., LATCHMAN J. L., STEWART R. C., WHITE, R. A & POWER J.  
1002 A. 1998. Soufrière Hills Eruption, Montserrat, 1995-1997: Volcanic earthquake locations and fault plane  
1003 solutions. *Geophysical Research Letters* **25** (18), 3397-3400.
- 1004
- 1005 BACHMANN O & DUNGAN M. A. 2002. Temperature-induced Al-zoning in hornblendes of the Fish Canyon  
1006 magma, Colorado. *American Mineralogist* **87** (8-9), 1062-1076.
- 1007 BACON C. R. 1986. Magmatic Inclusions in Silicic and Intermediate Volcanic-Rocks. *Journal of*  
1008 *Geophysical Research-Solid Earth and Planets* **91**(B6), 6091-6112.
- 1009
- 1010 BARCLAY J., HERD R. A., EDWARDS B. R., CHRISTOPHER T.E., KIDDLE E. J., PLAIL M. & DONOVAN A. 2010.  
1011 Caught in the act: Implications for the increasing abundance of mafic enclaves during the recent eruptive  
1012 episodes of the Soufrière Hills Volcano, Montserrat. *Geophysical Research Letters* **37**, L00E09,  
1013 doi:10.1029/2010GL042509.
- 1014
- 1015 BARCLAY J., RUTHERFORD M. J., CARROLL M. R., MURPHY M. D., DEVINE J. D., GARDNER J. & SPARKS R. S.  
1016 J. 1998. Experimental phase equilibria constraints on pre-eruptive storage conditions of the Soufrière  
1017 Hills magma. *Geophysical Research Letters* **25**(18), 3437-3440.
- 1018
- 1019 BÉDARD J.H. 2010. Parameterization of the Fe=Mg exchange coefficient ( $K_d$ ) between clinopyroxene and  
1020 silicate melts. *Chemical Geology*, **274** (3-4), 169-176.
- 1021
- 1022 BLUNDY J., CASHMAN K. & HUMPHREYS, M.C.S. 2006. Magma heating by decompression-driven  
1023 crystallization beneath andesite volcanoes. *Nature* **443**(7107) 76-80.
- 1024
- 1025 BLUNDY J. D. & HOLLAND T. J. B. 1990. Calcic Amphibole Equilibria and a New Amphibole-Plagioclase  
1026 Geothermometer. *Contributions to Mineralogy and Petrology* **104**(2) 208-224.
- 1027
- 1028 BOLGE L.L., CARR M.J., FEIGENSON M.D. & ALVARADO G.E. 2006. Geochemical stratigraphy and  
1029 magmatic evolution at Arenal Volcano, Costa Rica. *Journal of Volcanology and Geothermal Research*  
1030 **157** (1-3), 34-48.
- 1031
- 1032 BROWNE B.L., EICHELBERGER J.C. PATINO L.C., VOGEL T.A., UTO K. & HOSHIZUMI H. 2006. Magma  
1033 mingling as indicated by texture and Sr/Ba ratios of plagioclase phenocrysts from Unzen volcano, SW  
1034 Japan. *Journal of Volcanology and Geothermal Research* **154**(1-2) 103-116.
- 1035
- 1036 BUCKLEY V., SPARKS R. & WOOD B. 2006. Hornblende dehydration reactions during magma ascent at  
1037 Soufrière Hills Volcano, Montserrat. *Contributions to Mineralogy and Petrology* **151**, 121-140.



1038 CALDER E. S., LUCKETT R., SPARKS R. S. J & VOIGHT B. 2002. Mechanisms of lava dome instability and  
1039 generation of rock falls and pyroclastic flows at Soufrière Hills Volcano, Montserrat. *Geological Society,*  
1040 *London, Memoir*, **21** (1)173-190.  
1041  
1042 CASHMAN K. V. 1992. Groundmass crystallization of Mount St. Helens dacite, 1980-1986: a tool for  
1043 interpreting shallow magmatic processes. *Contributions to Mineralogy and Petrology* **109**, 431-449.  
1044  
1045 CHRISTOPHER T.E., EDMONDS M., HUMPHREYS M. C. S. & HERD R. A.2010. Volcanic gas emissions from  
1046 Soufrière Hills Volcano, Montserrat 1995-2009, with implications for mafic magma supply and  
1047 degassing. *Geophysical Research Letters* **37**, L00E04, doi: 10.1029/2009GL041325  
1048  
1049 CLYNNE M. A. 1999. A Complex Magma Mixing Origin for Rocks Erupted in 1915, Lassen Peak,  
1050 California. *Journal of Petrology* **40**(1), 105-132.  
1051  
1052 COUCH S., HARFORD C. L., SPARKS R. S. J. & CARROLL M. R. 2003a. Experimental Constraints on the  
1053 Conditions of Formation of Highly Calcic Plagioclase Microlites at the Soufriere Hills Volcano,  
1054 Montserrat. *Journal of Petrology* **44**(8), 1455-1475.  
1055  
1056 COUCH S., SPARKS R. S. J. & CARROLL M. R. 2003b. The Kinetics of Degassing-Induced Crystallization at  
1057 Soufrière Hills Volcano, Montserrat. *Journal of Petrology* **44**(8), 1477-1502.  
1058  
1059 DAVI M., BEHRENS H., VETERE F. & DE ROSA R. 2009. The viscosity of latitic melts from Lipari (Aeolian  
1060 Islands, Italy): Inference on mixing-mingling processes in magmas. *Chemical Geology* **259**(1-2), 89-97.  
1061  
1062 DEVINE J. D., GARDNER J. E., BRACK H. P., LAYNE G. D. & RUTHERFORD M. J. 1995. Comparison of  
1063 Microanalytical Methods for Estimating H<sub>2</sub>O Contents of Silicic Volcanic Glasses. *American*  
1064 *Mineralogist* **80**(3-4), 319-328.  
1065  
1066 DEVINE J. D., MURPHY M. D., RUTHERFORD M. J., BARCLAY J., SPARKS R. S. J., CARROLL M. R.,  
1067 YOUNG S. R. & GARDNER J. E. 1998a. Petrologic evidence for pre-eruptive pressure-temperature  
1068 conditions, and recent reheating, of andesitic magma erupting at the Soufrière Hills Volcano, Montserrat,  
1069 W.I. *Geophysical Research Letters* **25**(19), 3669-3672.  
1070  
1071 DEVINE J. D., RUTHERFORD M. J. & GARDNER J. E. 1998b. Petrologic determination of ascent rates for the  
1072 1995-1997 Soufrière Hills Volcano andesitic magma. *Geophysical Research Letters* **25**(19), 3673-3676.  
1073  
1074 DEVINE J. D., RUTHERFORD M. J., NORTON G. E. & YOUNG S. R. 2003. Magma Storage Region Processes  
1075 Inferred from Geochemistry of Fe-Ti Oxides in Andesitic Magma, Soufrière Hills Volcano, Montserrat,  
1076 W.I. *Journal of Petrology* **44**(8), 1375-1400.  
1077  
1078 DEVINE J. D. & RUTHERFORD M. J. this volume. Magma Storage Processes of the Soufrière Hills Volcano  
1079 Montserrat W.I. *Geological Society of London Memoir*, (The eruption of Soufrière Hills Volcano,  
1080 Montserrat from 2000 to 2010).  
1081  
1082 DUPUY C., DOSTAL J. & TRAINÉAU H.1985. Geochemistry of volcanic rocks from Mt. Pelée, Martinique.  
1083 *Journal of Volcanology and Geothermal Research* **26** (1-2), 147-165.  
1084  
1085 EDMONDS M., HUMPHREYS M.C.S., HARUI E., HERD R., WADGE G., RAWSON H., LEDDEN R., PLAIL M.,  
1086 BARCLAY J., AIUPPA A., CHRISTOPHER T.E., GIUDICE G. & GUIDA R. 2013. Pre-eruptive vapour and its role  
1087 in controlling eruption style and longevity at Soufrière Hills Volcano. *Geological Society of London*  
1088 *Memoir*, (The eruption of Soufrière Hills Volcano, Montserrat from 2000 to 2010).

1089 EDMONDS M., HERD R.A. & STRUTT M.H. 2006. Tephra deposits associated with a large lava dome  
1090 collapse, Soufrière Hills Volcano, Montserrat, 12-15 July 2003. *Journal of Volcanology and Geothermal*  
1091 *Research* **153** (3-4), 313-330.  
1092  
1093 EDMONDS M., PYLE D. & OPPENHEIMER C.2001. A model for degassing at the Soufrière Hills Volcano,  
1094 Montserrat, West Indies, based on geochemical data. *Earth and Planetary Science Letters* **186** (2), 159-  
1095 173.  
1096  
1097 EDWARDS B. R. & RUSSELL J. K. 1998. Time scales of magmatic processes: New insights from dynamic  
1098 models for magmatic assimilation *Geology* **26** (12), 1103-1106.  
1099  
1100 EICHELBERGER J. C. 1980. Vesiculation of Mafic Magma During Replenishment of Silicic Magma  
1101 Reservoirs. *Nature* **288**(5790), 446-450.  
1102  
1103 ELSWORTH D., MATTIOLI G., TARON J., VOIGHT B. & HERD R. 2008. Implications of Magma Transfer  
1104 between Multiple Reservoirs on Eruption Cycling. *Science* **322** (5899), 246-248.  
1105  
1106 ERNST W. G. & LIU J. 1998. Experimental phase-equilibrium study of Al- and Ti-contents of calcic  
1107 amphibole in MORB - A semiquantitative thermobarometer. *American Mineralogist* **83**(9-10), 952-969.  
1108  
1109 FICHAUT M., MARCELOT G. & CLOCCHIATTI R. 1989a. Magmatology of Mt. Pelée (Martinique, F.W.I.). II:  
1110 Petrology of gabbroic and dioritic cumulates. *Journal of Volcanology and Geothermal Research* **38**(1-2),  
1111 171-187.  
1112  
1113 FICHAUT M., MAURY R.C., TRAINÉAU H., WESTERCAMP D., JORON J.L., GOURGAUD A. & COULON C. 1989b.  
1114 Magmatology of Mt. Pelée (Martinique, F.W.I.). III: Fractional crystallization versus magma mixing.  
1115 *Journal of Volcanology and Geothermal Research* **38**(1-2), 189-213.  
1116  
1117 FOROOZAN R., ELSWORTH D., VOIGHT B. & MATTIOLI G. S. 2010. Dual reservoir structure at Soufrière Hills  
1118 Volcano inferred from continuous GPS observations and heterogeneous elastic modeling. *Geophysical*  
1119 *Research Letters* **37** L00E12, doi: 10.1029/2010GL042511.  
1120  
1121 FOROOZAN R., ELSWORTH D., VOIGHT B. & MATTIOLI G. S. 2011. Magmatic-metering controls the stopping  
1122 and restarting of eruptions. *Geophysical Research Letters* **38**, L05306, doi: 10.1029/2010GL046591.  
1123  
1124 GARCIA M. O. & JACOBSON S. S. 1979. Crystal clots, amphibole fractionation and the evolution of calc-  
1125 alkaline magmas. *Contributions to Mineralogy and Petrology* **69**, 319-327.  
1126  
1127 GENAREAU K. & CLARKE A. B. 2010. Heterogeneous clasts as windows into magma mingling at Soufrière  
1128 Hills volcano. *Geophysical Research Letters* **37**, L00E02, doi:10.1029/2009GL041968.  
1129  
1130 GOURGAUD A., FICHAUT M. & JORON J.L.1989. Magmatology of Mt. Pelee(Martinique, F.W.I.). I: Magma  
1131 mixing and triggering of the 1902 and 1929 Pelean nuees ardentes. *Journal of Volcanology and*  
1132 *Geothermal Research* **38** (1-2), 143-169.  
1133  
1134 GRASSET O. & ALBAREDE F. 1994. Hybridization of mingling magmas with different densities. *Earth and*  
1135 *Planetary Science Letters* **121**(3-4), 327-332.  
1136  
1137 HAMMARSTROM J. M. & ZEN E. A. 1986. Aluminum in Hornblende - an Empirical Igneous Geobarometer.  
1138 *American Mineralogist* **71**(11-12), 1297-1313.  
1139

1140 HAMMER J. E. & RUTHERFORD M. J. 2002. An experimental study of the kinetics of decompression-  
1141 induced crystallization in silicic melt. *Journal of Geophysical Research* **107**(B1), 2021.  
1142  
1143 HERD R.A., EDMONDS M. & BASS V. A. 2005. Catastrophic lava dome failure at Soufrière Hills Volcano,  
1144 Montserrat, 12-13 July 2003. *Journal of Volcanology and Geothermal Research* **148** (3-4), 234-252.  
1145  
1146 HIGGINS M. D. & ROBERGE J. 2003. Crystal Size Distribution of Plagioclase and Amphibole from  
1147 Soufrière Hills Volcano, Montserrat: Evidence for Dynamic Crystallization-Textural Coarsening Cycles.  
1148 *Journal of Petrology* **44**(8), 1401-1411.  
1149  
1150 HOLLISTER L. S., GRISSOM G. C., PETERS E. K., STOWELL H. H. & SISSON V. B. 1987. Confirmation of the  
1151 Empirical Correlation of Al in Hornblende with Pressure of Solidification of Calc-Alkaline Plutons.  
1152 *American Mineralogist* **72**(3-4), 231-239.  
1153  
1154 HUMPHREYS M. C. S., CHRISTOPHER T.E. & HARDS V. 2009a. Microlite transfer by disaggregation of mafic  
1155 inclusions following magma mixing at Soufrière Hills volcano, Montserrat. *Contributions to Mineralogy  
1156 and Petrology* **157**(5), 609-624.  
1157 HUMPHREYS M. C. S., EDMONDS M., BARCLAY J., PLAIL M., PARKES D. & CHRISTOPHER T.E. 2013. A new  
1158 method to quantify the real supply of mafic components to a hybrid andesite. *Contributions to  
1159 Mineralogy and Petrology* **165**, 191-215  
1160  
1161 HUMPHREYS M. C. S., EDMONDS M., CHRISTOPHER T.E. & HARDS V. 2009b. Chlorine variations in the  
1162 magma of Soufrière Hills Volcano, Montserrat: Insights from Cl in hornblende and melt inclusions.  
1163 *Geochimica et Cosmochimica Acta* **73**(19), 5693-5708.  
1164  
1165 HUMPHREYS M. C. S., EDMONDS M., CHRISTOPHER T.E. & HARDS V. 2010. Magma hybridisation and  
1166 diffusive exchange recorded in heterogeneous glasses from Soufrière Hills Volcano, Montserrat.  
1167 *Geophysical Research Letters* **37**, L00E06, doi: 10.1029/2009GL041926.  
1168  
1169 HUMPHREYS M. C. S., KEARNS S.L. & BLUNDY J.D. 2006. SIMS investigation of electron-beam damage to  
1170 hydrous, rhyolitic glasses: Implications for melt inclusion analysis. *American Mineralogist* **91**(4), 667-  
1171 679.  
1172  
1173 JOHNSON M. C. & RUTHERFORD M.J. 1989. Experimental Calibration of the Aluminum-in-Hornblende  
1174 Geobarometer with Application to Long-Valley Caldera (California) Volcanic-Rocks. *Geology* **17**(9),  
1175 837-841.  
1176  
1177 KOMOROWSKI J. C., LEGENDRE Y., CHRISTOPHER T.E., BERNSTEIN M., STEWART R., JOSEPH E., FOURNIER N.,  
1178 CHARDOT L., FINIZOLA A., WADGE G., SYERS R., WILLIAMS C. & BASS V. 2010. Insights into processes and  
1179 deposits of hazardous vulcanian explosions at Soufrière Hills Volcano during 2008 and 2009 (Montserrat,  
1180 West Indies). *Geophysical Research Letters* **37**, L00E19,doi:10.1029/2010GL042558.  
1181  
1182 KUSHIRO I. 1960. Si-Al relation in clinopyroxenes from igneous rocks. *American Journal of Science*. **258**  
1183 (8), 548-554.  
1184  
1185 LINDSLEY D. H. (1983). Pyroxene Thermometry. *American Mineralogist* **68**(5-6), 477-493.  
1186  
1187 MARTEL C., RADADI A.A., POUSSINEAU S., GOURGAUD A. & PICHAVANT M. 2006. Basalt-inherited  
1188 microlites in silicic magmas: Evidence from Mount Pelée (Martinique, French West Indies). *Geology* **34**  
1189 (11), 905-908.  
1190

- 1191 MILLER A. D., STEWART R. C., WHITE R. A., LUCKETT R., BAPTIE B. J., ASPINALL W. P., LATCHMAN J. L.,  
1192 LYNCH L. L. & VOIGHT B. 1998. Seismicity associated with dome growth and collapse at the Soufrière  
1193 Hills Volcano, Montserrat. *Geophysical Research Letters* **25** (18), 3401-3404.  
1194
- 1195 MURPHY M. D., SPARKS R. S. J., BARCLAY J., CARROLL M. R. & BREWER T. S. 2000. Remobilization of  
1196 andesite magma by intrusion of mafic magma at the Soufrière Hills Volcano, Montserrat, West Indies.  
1197 *Journal of Petrology* **41**(1), 21-42.  
1198
- 1199 MURPHY M. D., SPARKS R. S. J., BARCLAY J., CARROLL M. R., LEJEUNE A. M., BREWER T. S., MACDONALD  
1200 R., BLACK S. & YOUNG S. 1998. The role of magma mixing in triggering the current eruption at the  
1201 Soufrière Hills volcano, Montserrat, West Indies. *Geophysical Research Letters* **25**(18), 3433-3436.  
1202
- 1203 NEWMAN S. & LOWENSTERN J.B. 2002. VolatileCalc: a silicate melt-H<sub>2</sub>O-CO<sub>2</sub> solution model written in  
1204 Visual Basic for excel. *Computers & Geosciences* **28**(5), 597-604.  
1205
- 1206
- 1207 NORTON G. E., WATTS R. B., VOIGHT B., MATTIOLI G. S., HERD R. A., YOUNG S. R., DEVINE J.D.,  
1208 ASPINNALL W. P., BONADONNA C., BAPTIE B. J., EDMONDS M., JOLLY A. D., LOUGHLIN S. C., LUCKETT R.  
1209 & SPARKS S. J. 2002. Pyroclastic flow and explosive activity at Soufrière Hills Volcano, Montserrat,  
1210 during a period of virtually no magma extrusion (March 1998 to November 1999). *Geological Society,*  
1211 *London, Memoir* **21** (1), 467-481.  
1212
- 1213 ODBERT H.M., STEWART R.C. & WADGE G. this volume. Cyclic Phenomena at the Soufrière Hills  
1214 Volcano, Montserrat. *Geological Society of London Memoir*, (The eruption of Soufrière Hills Volcano,  
1215 Montserrat from 2000 to 2010).
- 1216 PERUGINI D. & POLI G. 2005. Viscous fingering during replenishment of felsic magma chambers by  
1217 continuous inputs of mafic magmas: Field evidence and fluid-mechanics experiments. *Geology* **33** (1), 5-  
1218 8.  
1219
- 1220 PICHAVANT M., COSTA F., BURGISSER A., SCAILLET B., MARTEL C. & POUSSINEAU S. 2007. Equilibration  
1221 Scales in Silicic to Intermediate Magmas-Implications for Experimental Studies. *Journal of Petrology* **48**  
1222 (10), 1955-1972.  
1223
- 1224 PICHAVANT M., MARTEL C., BOURDIER J.L. & SCAILLET B. 2002. Physical conditions, structure, and  
1225 dynamics of a zoned magma chamber: Mount Pelée (Martinique, Lesser Antilles Arc). *Journal of*  
1226 *Geophysical Research: Solid Earth*. **105 B5**, doi - 10.1029/2001JB000315.  
1227
- 1228 PLAIL M., BARCLAY J., HUMPHREYS M. C. S., EDMONDS M., HERD R.A. & CHRISTOPHER T.E. this volume.  
1229 Characterisation of mafic enclaves in the erupted products of Soufrière Hills Volcano, Montserrat 1995-  
1230 2010. *Geological Society of London Memoir*, (The eruption of Soufrière Hills Volcano, Montserrat from  
1231 2000 to 2010).  
1232
- 1233 PLECHOV P., TSAI A., SHCHERBAKOV V. & DIRKSEN O. 2008. Opacitization conditions of hornblende in  
1234 Bezymyanni volcano andesites (March 30, 1956 eruption). *Petrology* **16** (1), 19-35.  
1235
- 1236 PUTIRKA K.D. 1999. Clinopyroxene plus liquid equilibria to 100 kbar and 2450 K. *Contributions to*  
1237 *Mineralogy and Petrology* **135**(2-3), 151-163.  
1238
- 1239 PUTIRKA K. D. 2005. Igneous thermometers and barometers based on plagioclase + liquid equilibria: Tests  
1240 of some existing models and new calibrations. *American Mineralogist* **90**(2-3), 336-346.

1241 PUTIRKA K.D., JOHNSON M., KINZLER R., LONGHI J. & WALKER D. 1996. Thermobarometry of mafic  
1242 igneous rocks based on clinopyroxene-liquid equilibria, 0-30 kbar. *Contributions to Mineralogy and*  
1243 *Petrology* **123**(1), 92-108.  
1244  
1245 PUTIRKA K. D., MIKAELIAN H., RYERSON F. & SHAW H. 2003. New clinopyroxene-liquid  
1246 thermobarometers for mafic, evolved, and volatile-bearing lava compositions, with applications to lavas  
1247 from Tibet and the Snake River Plain, Idaho. *American Mineralogist* **88**(10), 1542-1554.  
1248  
1249 REAGAN M. K., GILL J.B., MALAVASSI E. & GARCIA M.O. 1987. Changes in magma composition at Arenal  
1250 volcano, Costa Rica, 1968-1985: Real-time monitoring of open-system differentiation. *Bulletin of*  
1251 *Volcanology* **49**, 415-434.  
1252  
1253 RHODES J.M. & DUNGAN M.A. 1977. The nature of primary ocean floor basalts. Papers presented to the  
1254 second inter-team meeting, *Basaltic volcanism study project*. 50-52. Lunar Science Institute, Huston.  
1255  
1256 RIDOLFI F., RENZULLI A. & PUERINI M. 2010. Stability and chemical equilibrium of amphibole in calc-  
1257 alkaline magmas: an overview, new thermobarometric formulations and application to subduction-related  
1258 volcanoes. *Contributions to Mineralogy and Petrology* **160**(1), 45-66.  
1259  
1260 ROBERTSON R. E. A., ASPINALL W. P., HERD R. A., NORTON G. E., SPARKS R. S. J. & YOUNG, S. R. 2000.  
1261 The 1995-1998 eruption of the Soufrière Hills volcano, Montserrat, WI. *Philosophical Transactions of*  
1262 *the Royal Society of London Series A-Mathematical Physical and Engineering Sciences* **358** (1770) 1619-  
1263 1637.  
1264  
1265 RUTHERFORD M. J. & DEVINE J. D. 2003. Magmatic Conditions and Magma Ascent as Indicated by  
1266 Hornblende Phase Equilibria and Reactions in the 1995-2002 Soufrière Hills Magma. *Journal of*  
1267 *Petrology* **44**(8), 1433-1453.  
1268  
1269 RUTTER M. J., VANDERLAAN S. R. & WYLLIE P. J. 1989. Experimental-Data for a Proposed Empirical  
1270 Igneous Geobarometer - Aluminum in Hornblende at 10 Kbar Pressure. *Geology* **17**(10): 897-900.  
1271  
1272 RYDER C.H., GILL J.B., TEPLY III F., RAMOS F. & REAGAN M. 2006. Closed- to open-system  
1273 differentiation at Arenal volcano (1968-2003). *Journal of Volcanology and Geothermal Research* **157** (1-  
1274 3), 75-93.  
1275  
1276 SAITO G., KOHEI K. & HIROSHI S. 2003. Volatile evolution of Satsuma-Iwojima volcano: Degassing  
1277 process and mafic-felsic magma interaction. *Developments in Volcanology Melt Inclusions in Volcanic*  
1278 *Systems - Methods, Applications and Problems* **5**, 129-146.  
1279  
1280 SCHMIDT M. W. 1992. Amphibole composition in tonalite as a function of pressure: an experimental  
1281 calibration of the Al-in-hornblende barometer. *Contributions to Mineralogy and Petrology* **110**(2), 304-  
1282 310.  
1283  
1284 SCHUMACHER J. C. 1997. The estimation of ferric iron in electron microprobe analysis of amphiboles.  
1285 *Mineralogical Magazine* **61**, 312-321.  
1286  
1287 SHEPHERD J., TOMBLIN J. & WOO D. 1971. Volcano-seismic crisis in Montserrat, West Indies, 1966-67.  
1288 *Bulletin of Volcanology* **35**, 143-162.  
1289  
1290 SHINOHARA H. 2008. Excess Degassing from Volcanoes and Its Role on Eruptive and Intrusive Activity.  
1291 *Reviews of Geophysics* **46** (4). WOS:000260997900001.

1292 SNYDER D. 2000. Thermal effects of the intrusion of basaltic magma into a more silicic magma chamber  
1293 and implications for eruption triggering. *Earth and Planetary Science Letters* **175**(3-4), 257-273.  
1294  
1295 SNYDER D. & TAIT S. 1995. Replenishment of magma chambers: comparison of fluid-mechanic  
1296 experiments with field relations. *Contributions to Mineralogy and Petrology* **122** (3), 230-240.  
1297  
1298 SNYDER, D. & TAIT S. 1998a. A flow-front instability in viscous gravity currents. *Journal of Fluid*  
1299 *Mechanics* **369**, 1-21.  
1300  
1301 SNYDER, D. & TAIT S. 1998b. The imprint of basalt on the geochemistry of silicic magmas. *Earth and*  
1302 *Planetary Science Letters* **160**(3-4), 433-445.  
1303  
1304 SPARKS, R. S. J. & MARSHALL L. A. 1986. Thermal and mechanical constraints on mixing between mafic  
1305 and silicic magmas. *Journal of Volcanology and Geothermal Research* **29**(1-4), 99-124.  
1306 STINTON A.J., COLE P. D., ODBERT H.M., CHRISTOPHER T.E, AVARD G. & BERNSTEIN M. 2013. Evolution  
1307 of the Soufrière Hills volcano during a short, intense episode of dome growth: 4 October 2009 - 11  
1308 February 2010. *Geological Society of London Memoir*, (The eruption of Soufrière Hills Volcano,  
1309 Montserrat from 2000 to 2010).  
1310  
1311 STORMER J. C. 1983. The Effects of Recalculation on Estimates of Temperature and Oxygen Fugacity  
1312 from Analyses of Multicomponent Iron Titanium-Oxides. *American Mineralogist* **68**(5-6), 586-594.  
1313  
1314 STRECK M., DUNGAN M., MALAVASSI E. M., REAGAN M. & BUSSY F. 2002. The role of basalt  
1315 replenishment in the generation of basaltic andesites of the ongoing activity at Arenal volcano, Costa  
1316 Rica: evidence from clinopyroxene and spinel. *Bulletin of Volcanology* **64** (5), 316-327.  
1317  
1318 THOMAS N. & TAIT S.R. 1997. The dimensions of magmatic inclusions as a constraint on the physical  
1319 mechanism of mixing. *Journal of Volcanology and Geothermal Research* **75** (1-2), 167-178.  
1320  
1321 THOMAS N., TAIT S. & KOYAGUCHI T. 1993. Mixing of stratified liquids by the motion of gas bubbles:  
1322 application to magma mixing. *Earth and Planetary Science Letters* **115**(1-4), 161-175.  
1323  
1324 TONARINI S., ARMIENTI P., D'ORAZIO M., INNOCENTI F., POMPILIO M. & PETRINI R. 1995. Geochemical and  
1325 isotopic monitoring of Mt Etna 1989-1993 eruptive activity: bearing on the shallow feeding system.  
1326 *Journal of Volcanology and Geothermal Research*, **64**, 95-115.  
1327  
1328 TRAIL A. F. & SPERA F.J. 1990. Mechanisms for the generation of compositional heterogeneities in  
1329 magma chambers. *Geological Society of America Bulletin* **102** (3), 353-367.  
1330  
1331 WADGE G., HERD R., RYAN G., CALDER E. S. & KOMOROWSKI J.C. 2010. Lava production at Soufrière  
1332 Hills Volcano, Montserrat: 1995-2009. *Geophysical. Research Letters* **37**, doi- 10.1029/2009GL041466.  
1333  
1334 WADGE G. & ISAACS M. C. 1988. Mapping the Volcanic Hazards from Soufrière Hills Volcano,  
1335 Montserrat, West Indies Using an Image Processor. *Journal of the Geological Society* **145**, 541-552.  
1336  
1337 YOUNG S., SPARKS R.S.J., ASPINALL W.P., LYNCH L.L., MILLER A.D., ROBERTSON R.E.A. & SHEPHERD J.B.  
1338 1998. Overview of the eruption of Soufrière Hills Volcano, Montserrat, 18 July 1995 to December 1997.  
1339 *Geophysical. Research Letters* **25** (18) 3389-3392.  
1340

1341 ZELLMER G. F., HAWKESWORTH C. J., SPARKS R. S. J., THOMAS L. E., HARFORD C. L., BREWER T. S. &  
1342 LOUGHLIN S. C. 2003a. Geochemical Evolution of the Soufrière Hills Volcano, Montserrat, Lesser  
1343 Antilles Volcanic Arc. *Journal of Petrology* **44**(8), 1349-1374.  
1344  
1345 ZELLMER G. F., SPARKS R.S.J., HAWKESWORTH C. J. & WIEDENBECK M. 2003b. Magma Emplacement and  
1346 Remobilization Timescales Beneath Montserrat: Insights from Sr and Ba Zonation in Plagioclase  
1347 Phenocrysts. *Journal of Petrology* **44**(8), 1413-1431.  
1348  
1349  
1350  
1351  
1352  
1353  
1354  
1355  
1356  
1357  
1358  
1359  
1360  
1361  
1362  
1363  
1364  
1365  
1366  
1367  
1368  
1369  
1370  
1371  
1372  
1373  
1374  
1375  
1376  
1377  
1378  
1379  
1380  
1381  
1382  
1383  
1384  
1385  
1386  
1387  
1388  
1389  
1390  
1391

## Figure captions

1392  
1393  
1394  
1395 Figure 1 Box plots showing relative plagioclase An contents by eruption phase for andesite phenocryst  
1396 rims A, andesite microlites B, sieved rims, oscillatory rims and enclave crystals C, phenocryst cores by  
1397 texture D. Microlite Fe content vs An content by phase E, Fe content vs An content for sieve and enclave  
1398 crystals F.

1399  
1400 Figure 2 Typical andesite whole rock texture found in Phases IV and V. pl – plagioclase, px-  
1401 orthopyroxene, cpx- clinopyroxene, ox- Fe-Ti oxide.

1402  
1403 Figure 3 Examples of enclave textures described by Plail et al (this volume). P- plagioclase, Px –  
1404 clinopyroxene, Hbl – hornblende, Ox – Fe-Ti oxides, V – vesicles

1405  
1406 Figure 4 Amphibole compositions in andesite and enclaves by phase A, box plots for mg#'s of amphibole  
1407 phenocryst rims in the andesite B, enclaves by phase and mg# C, enclaves by phase and Fe content D. an-  
1408 andesite, en- enclaves. The number of analyses used is given in each box, horizontal line represents  
1409 median values.

1410  
1411 Figure 5 Box plots of mg# for andesite orthopyroxene unzoned rims (by phase) and rev-zoned rims A,  
1412 andesite orthopyroxene microlites (by phase) and enclave microlites B, bulk rock total alkali by eruption  
1413 phase C, andesite hosted clinopyroxene microlite Kd values by phase D. The number of analyses used is  
1414 given in each box, horizontal line represents median values. an – andesites, en- enclaves.

1415  
1416 Figure 6 Abundances of major elements in andesite and enclave glass from microprobe analyses,  
1417 andesites- An, enclaves- En. High  $K_2O > 3wt\%$ , low  $K_2O < 3wt\%$ .

1418 Figure 7 Bulk andesite and enclave major element abundances by phase, vertical dashed line demarcates  
1419 boundary between silica content of the andesite- An, enclave- En.

1420  
1421 Figure 8 Box plots showing inter-phase bulk rock contents of FeO, V, Ba and plagioclase microlite Fe  
1422 content throughout the eruption. The number of analyses used is given in each box, horizontal line  
1423 represents median values, mic- microlite, an – andesites, en- enclaves.



1424 Figure 9 Selected trace element plots for bulk rock andesite and enclave products. Symbols and labels are  
1425 the same as Figure 7, vertical line demarcates boundary between andesite and enclave silica content.

1426  
1427 Figure 10 Major element behaviour with changing FeO/MgO showing changes as function of crystal  
1428 control. Arrows indicate removal of particular mineral phase. An- andesite, En – enclaves. Fractionation  
1429 and assimilation vectors for the other oxides are same as in Al<sub>2</sub>O<sub>3</sub>.

1430  
1431 Figure 11 Harker plots of SiO<sub>2</sub> vs FeO for phases I, II and III by lab showing an absence of any  
1432 systematic inter-lab variation in the data for andesites- A and enclaves-B. L-leicester, JD- Joe Devine, SS-  
1433 (Murphy et al., 1998), BGS- British geological survey, UEA- University of East Anglia, MGU- Mc Gill  
1434 University.

1435

1436

1437

1438

#### Table captions

1439 Table 1 Laboratory and sample information for the XRF data used in this study; An-andesite, En- enclave.

1440

1441 Table 2 Published modal mineral contents for the first three extrusion phases. Arbitrary distinction  
1442 between microlites and microphenocryst defined by 100µm, \*Recalculated from point counts in  
1443 Humphreys et al., 2009a, range shown.

1444

1445 Table 3 Mineral phases and associated textures in the andesite and enclave lavas of the current eruption.

1446

1447 Table 4 Averaged andesite plagioclase phenocryst and microlite microprobe data, comparing  
1448 compositions from Phases IV and V with the published compositions of Phases I, II and III. pc-  
1449 phenocryst core, pr - phenocryst rim, mc- microlite core, mr- microlite rim, mpc- microphenocryst core,  
1450 mpr – microphenocryst rim, An- andesite, En – enclave.

1451

1452 Table 5a Averaged andesite amphibole compositions by texture and eruption phase.

1453

1454 Table 5b Averaged enclave amphibole compositions from eruption Phases I, II, III and V along side high  
1455 aluminum andesite hosted microphenocrysts and groundmass fragments. Mphx – microphenocrysts, Frag  
1456 – groundmass fragments. Phase V data from Plail et al. (this volume)

1457

1458 Table 6a Averaged Orthopyroxene phenocryst and microlite compositions comparing the andesite  
1459 crystals of phase IV and V with crystals from phases I, II and III , errors are  $\pm 1\sigma$ , mic – microlites, phx-  
1460 phenocrysts.

1461

1462 Table 6b Averaged compositions of andesite hosted reverse zoned orthopyroxene phenocryst rims along  
1463 with andesite and enclave microphenocrysts, errors are  $\pm 1\sigma$ , Mphx- microphenocrysts, Phx- phenocrysts

1464

1465 Table 6c Averaged compositions of clinopyroxene microphenocrysts, microlites and overgrowths, errors  
1466 are  $\pm 1\sigma$ , mic – microlites, mphx- microphenocrysts.

1467

1468 Table 7a Averaged andesite titanomagnetite compositions, sorted by eruptive phase and textural type.  
1469 Usp/Ilm mol% after Stormer (1983), mic – microlites.

1470

1471 Table 7b Averaged compositions of enclave oxides along with andesite derived ilmenite.

1472

1473 Table 8 Averaged microprobe glass compositions for andesites and enclaves, along with  $\log f_{O_2}$  values  
1474 from touching ilmenite–magnetite pairs.

1475

1476 Table 9 Averaged bulk rock major element compositions for the andesite and enclaves of the different  
1477 eruption phases.

1478

1479 Table 10 Averaged bulk rock trace element for andesites and enclaves of the different eruption phases.

1480

1481 Table 11 Temperature and Pressure estimates for the eruptive products obtained using a number of  
1482 different techniques.

1483

1484 Table 12 Intra-phase andesite mass balance calculations for addition of enclave crystals, weight % values  
1485 are relative to initial magma compositions.

1486

1487

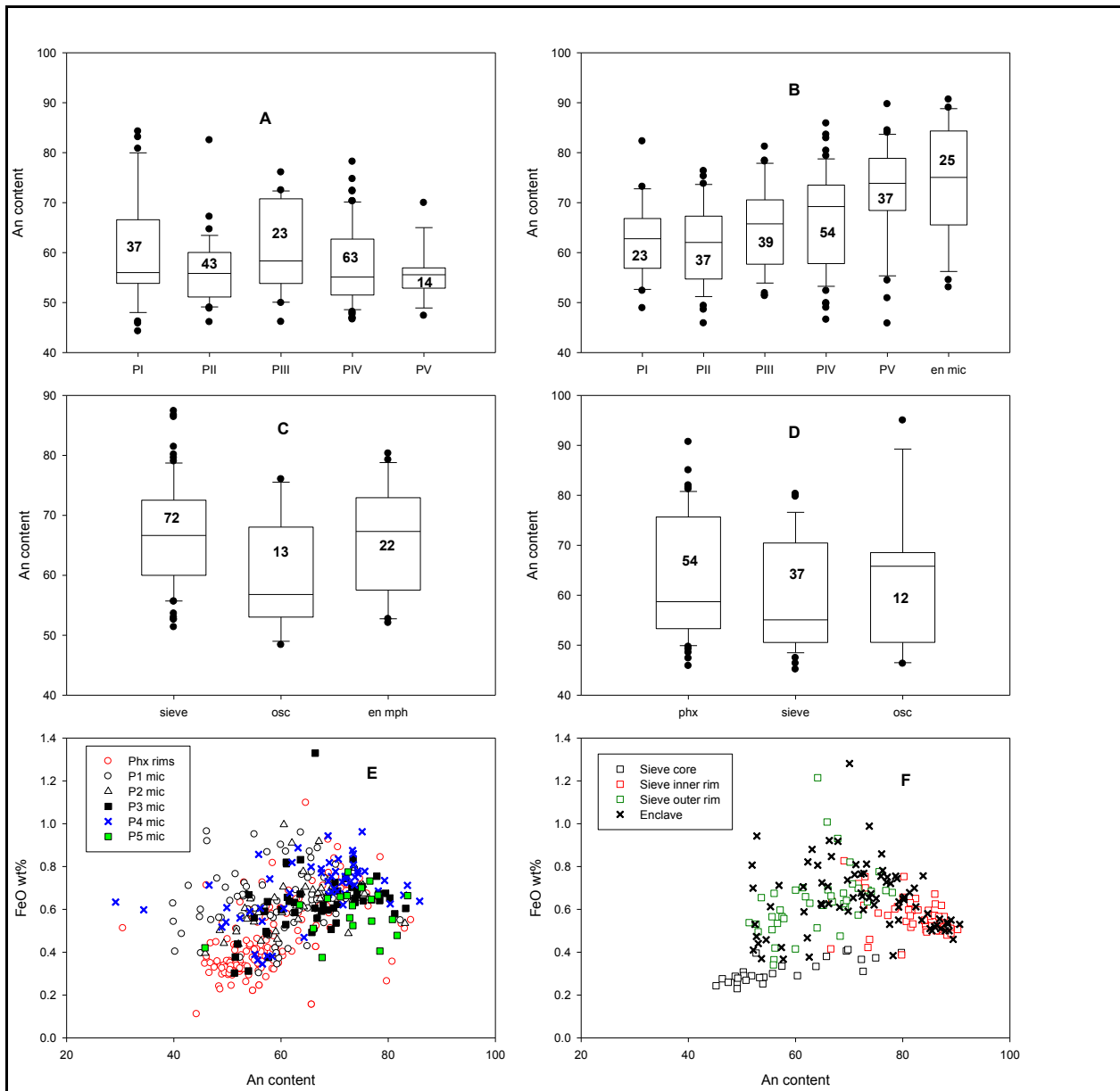


Figure 1 Box plots showing relative plagioclase An contents by eruption phase for andesite phenocryst rims A, andesite microlites B, sieved rims, oscillatory rims and enclave crystals C, phenocryst cores by texture D. Microlite Fe content vs An content by phase E, Fe content vs An content for sieve and enclave crystals F.

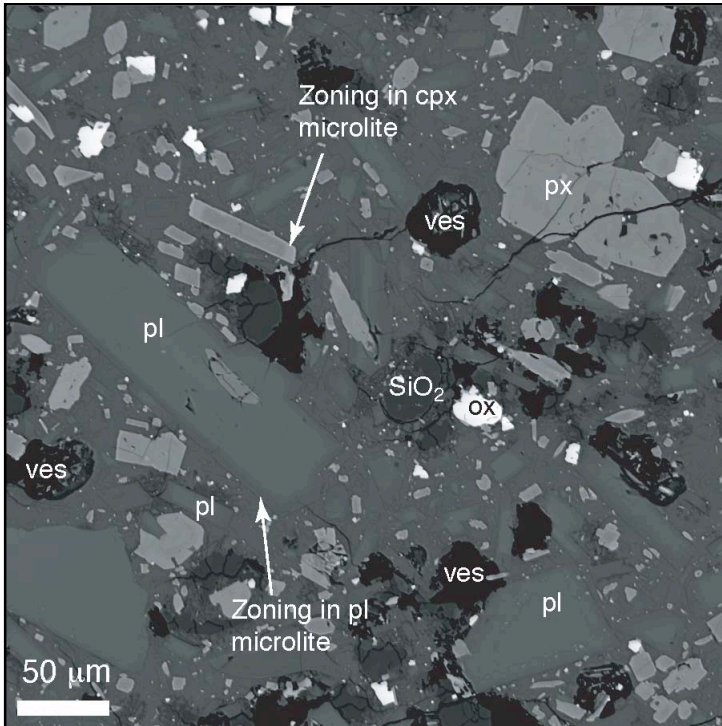


Figure 2 Typical andesite whole rock texture found in Phases IV and V.  
pl – plagioclase, px- orthopyroxene, cpx- clinopyroxene, ox- Fe-Ti oxide.

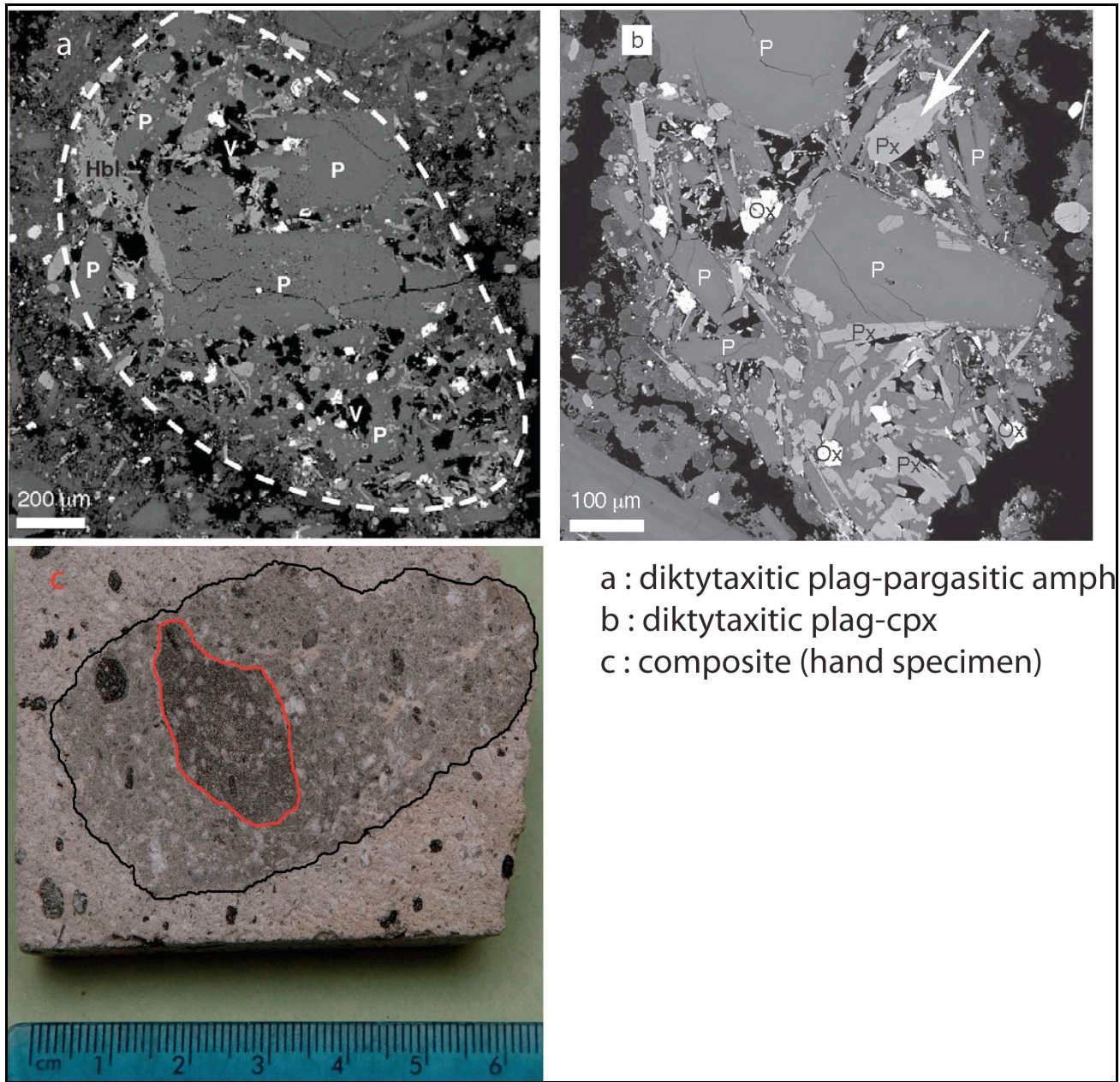


Figure 3 Examples of enclave textures described by Plail et al (this volume). P- plagioclase, Px – clinopyroxene, Hbl – hornblende, Ox – Fe-Ti oxides, V – vesicles

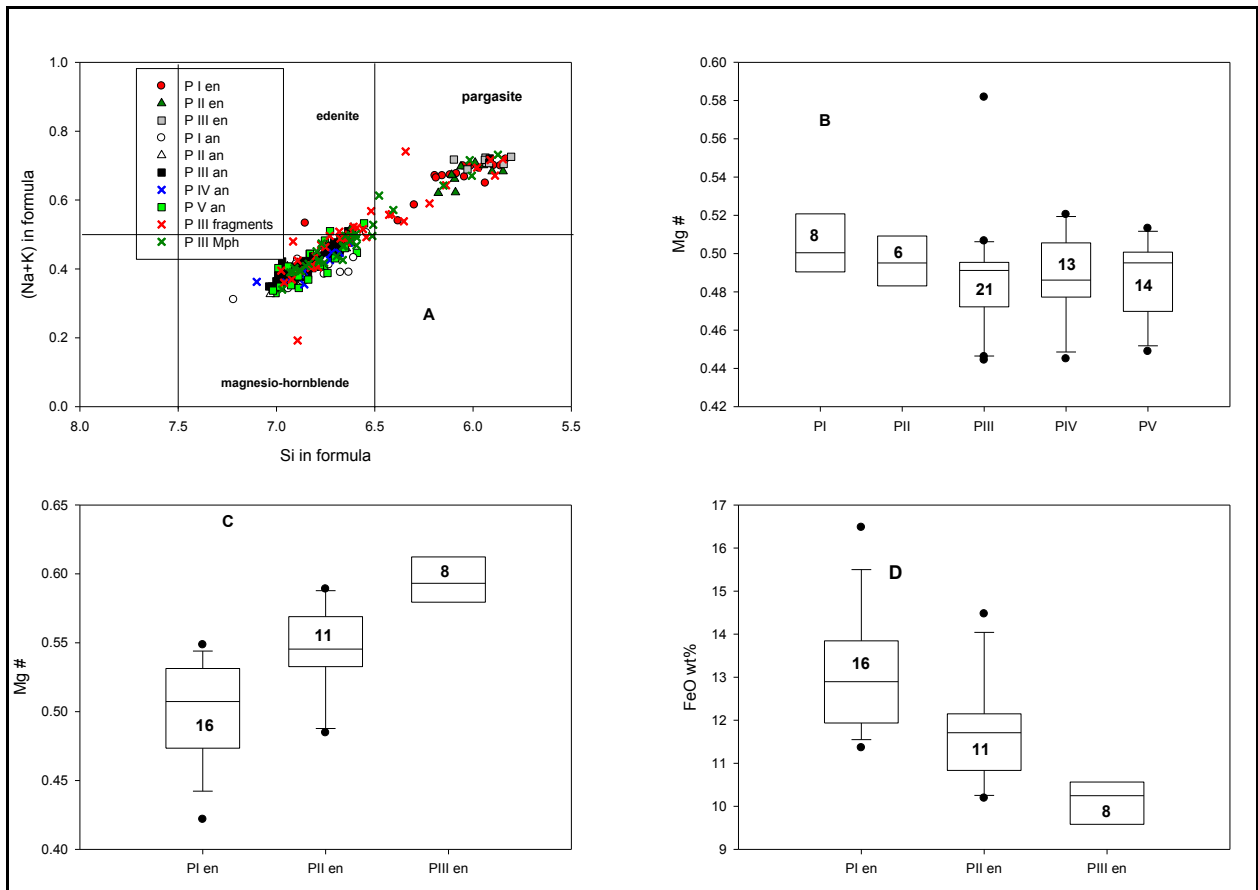


Figure 4 Amphibole compositions in andesite and enclaves by phase A, box plots for mg#s of amphibole phenocryst rims in the andesite B, enclaves by phase and mg# C, enclaves by phase and Fe content D. an-andesite, en- enclaves. The number of analyses used is given in each box, horizontal line represents median values.

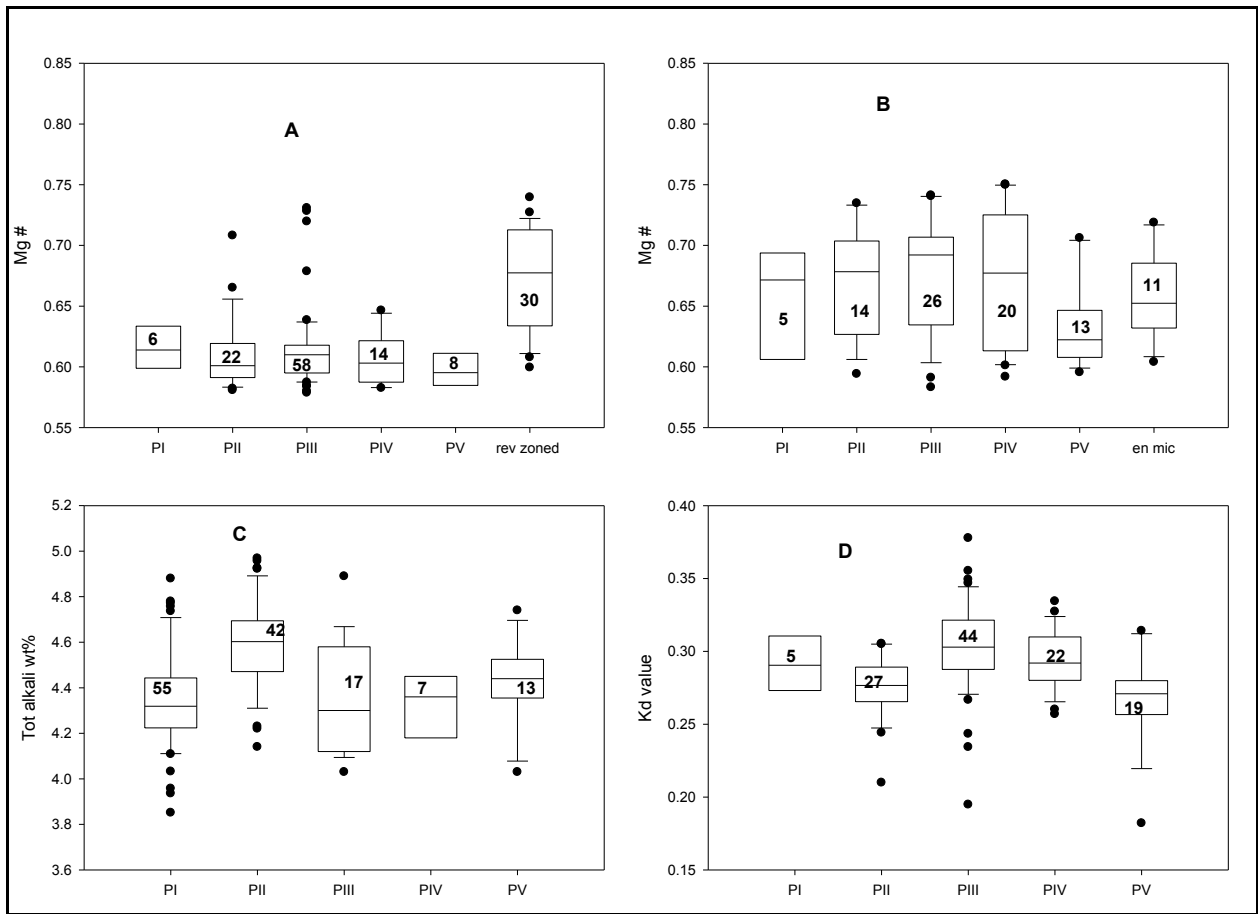


Figure 5 Box plots of mg# for andesite orthopyroxene unzoned rims (by phase) and rev-zoned rims A, andesite orthopyroxene microlites (by phase) and enclave microlites B, bulk rock total alkali by eruption phase C, andesite hosted clinopyroxene microlite Kd values by phase D. The number of analyses used is given in each box, horizontal line represents median values. an – andesites, en- enclaves.



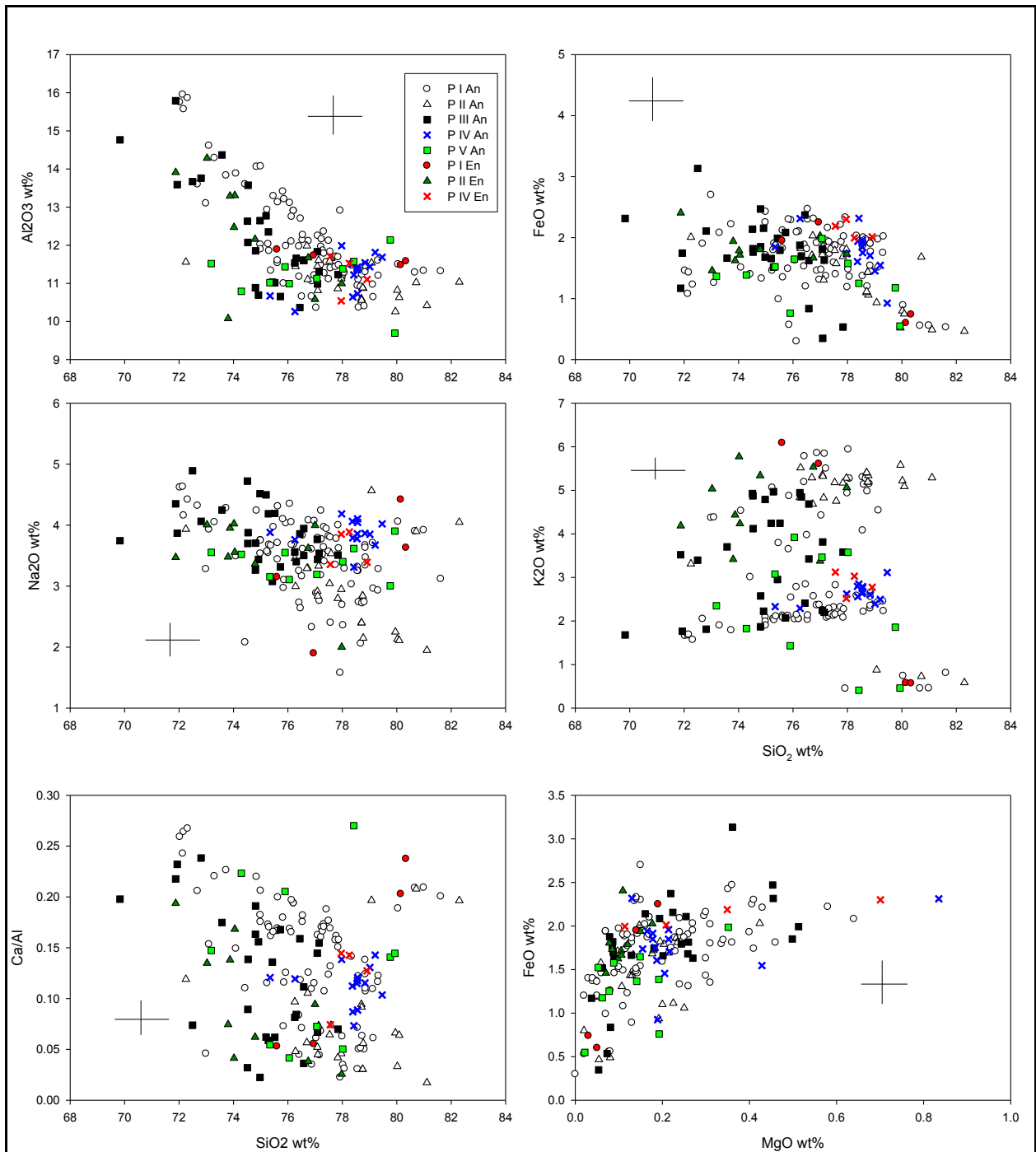


Figure 6 Abundances of major elements in andesite and enclave glass from microprobe analyses, andesites- An, enclaves- En. High K<sub>2</sub>O > 3wt%, low K<sub>2</sub>O < 3wt%.

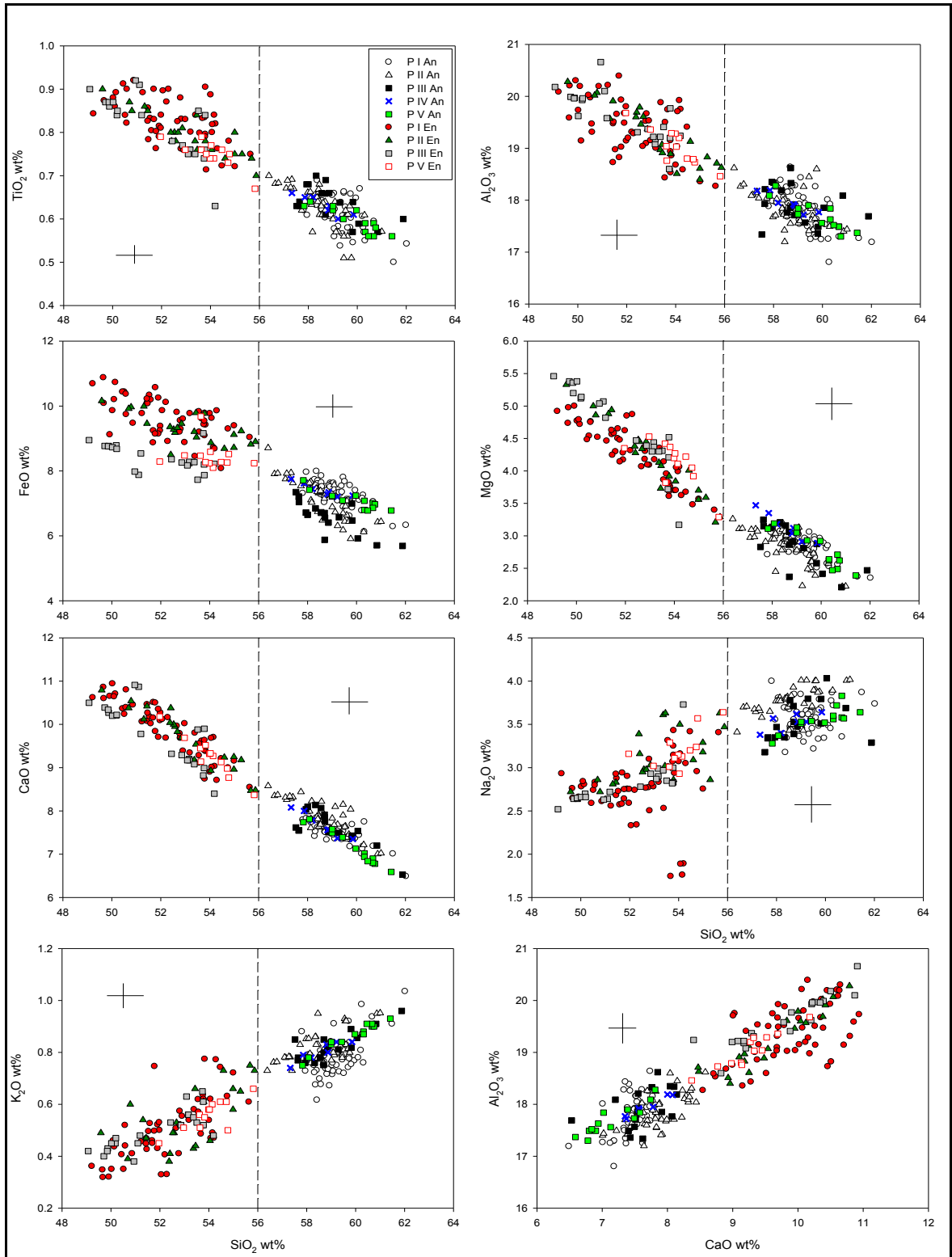


Figure 7 Bulk andesite and enclave major element abundances by phase, vertical dashed line demarcates boundary between silica content of the andesite- An, enclave- En.

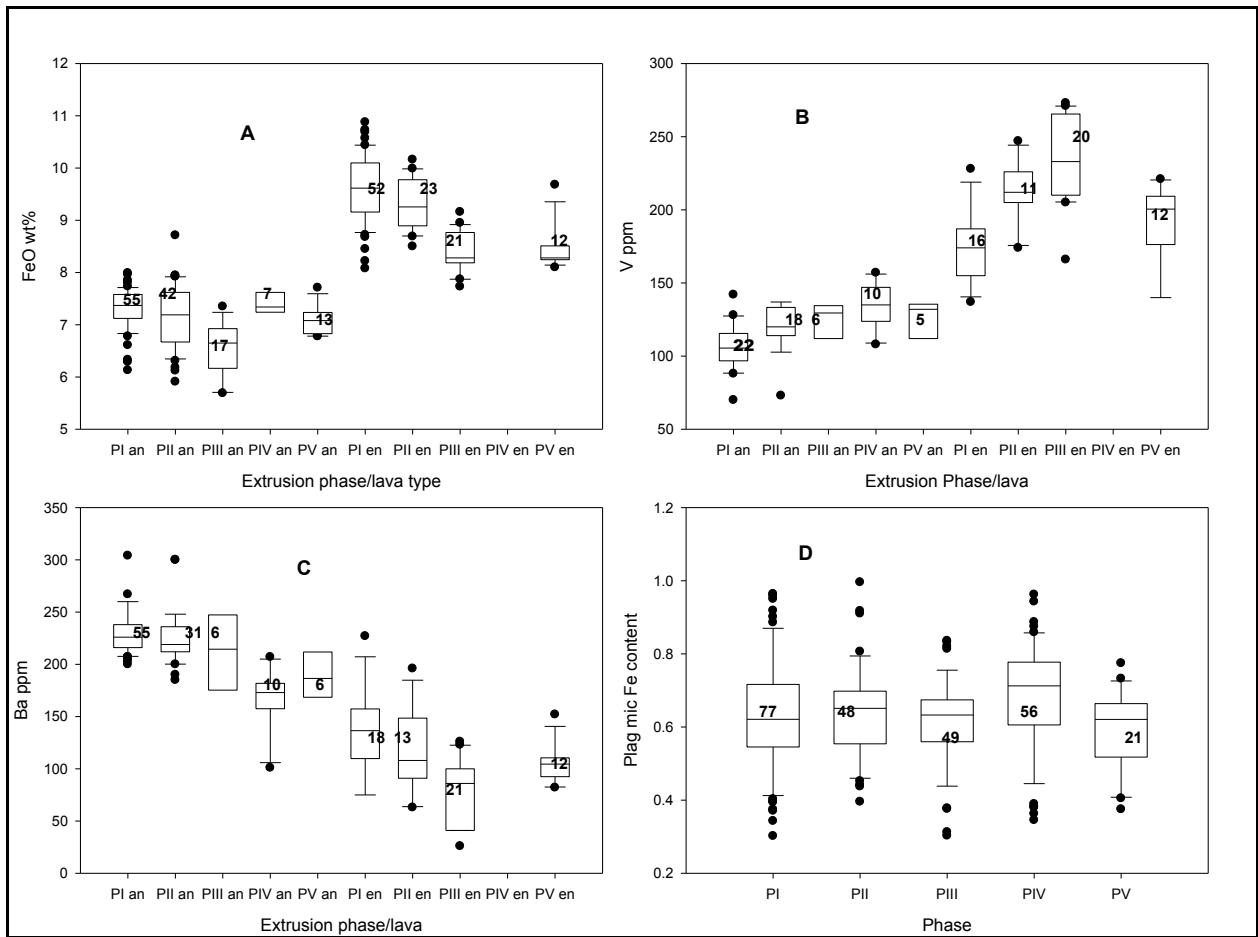


Figure 8 Box plots showing inter-phase bulk rock contents of FeO, V, Ba and plagioclase microlite Fe content throughout the eruption. The number of analyses used is given in each box, horizontal line represents median values, mic- microlite, an – andesites, en- enclaves.

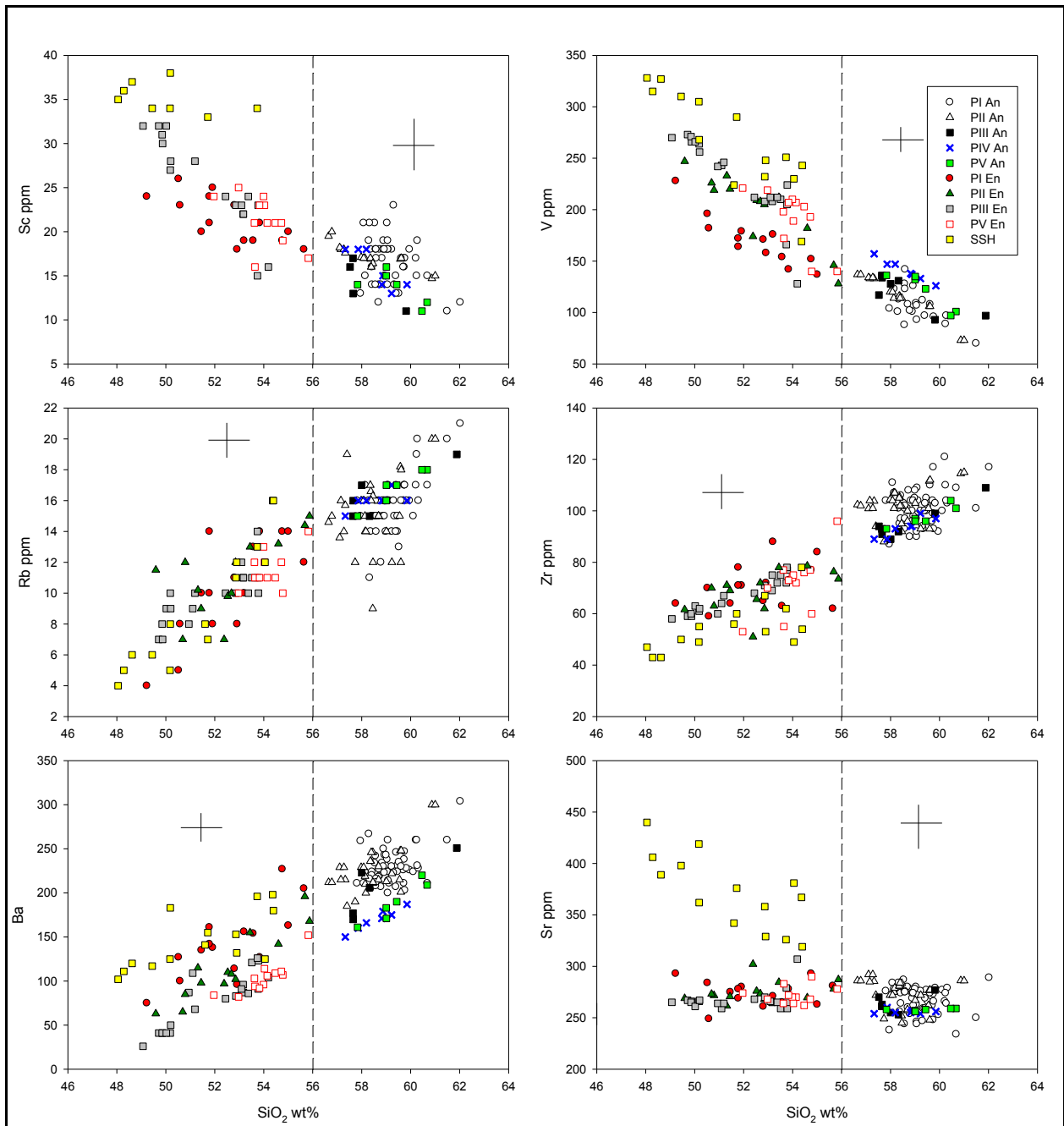


Figure 9 Selected trace element plots for bulk rock andesite and enclave products. Symbols and labels are the same as Figure 7, vertical line demarcates boundary between andesite and enclave silica content.

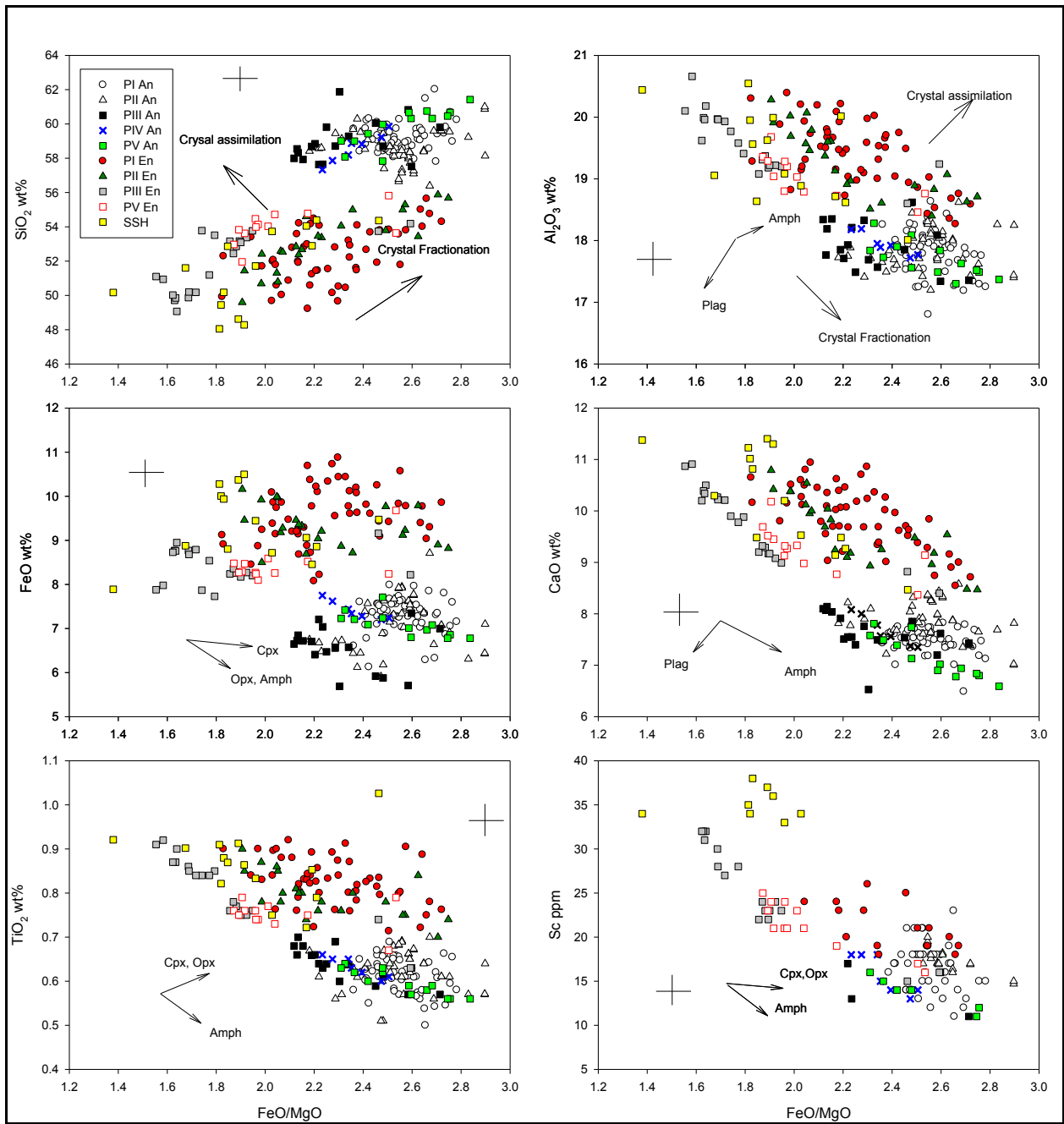


Figure 10 Major element behaviour with changing FeO/MgO showing changes as function of crystal control. Arrows indicate removal of particular mineral phase. An- andesite, En – enclaves. Fractionation and assimilation vectors for the other oxides are same as in  $Al_2O_3$ .

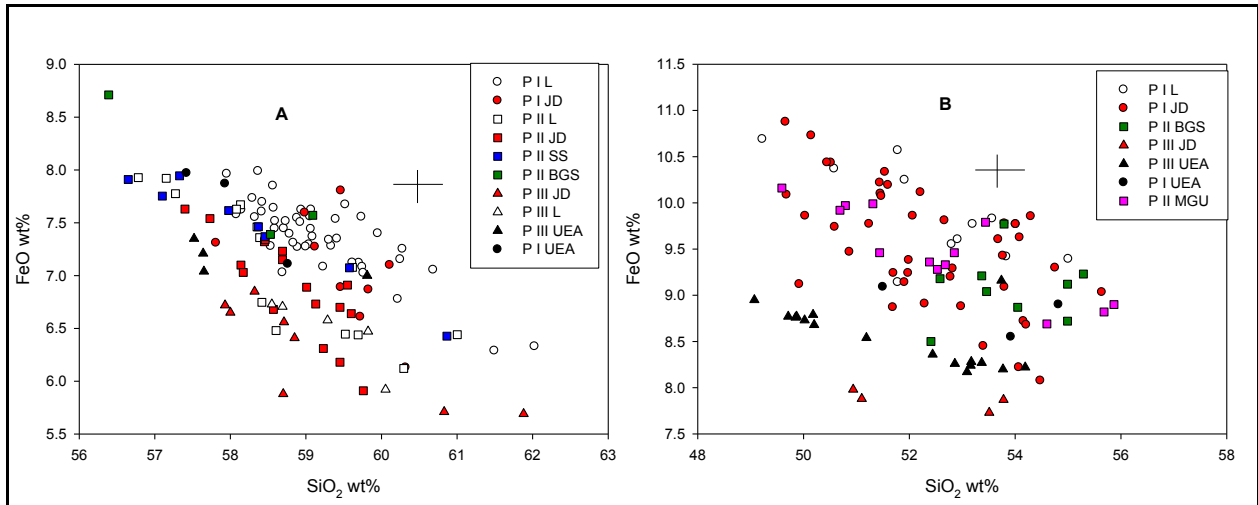


Figure 11 Harker plots of  $\text{SiO}_2$  vs FeO for phases 1, II and III by lab showing an absence of any systematic inter-lab variation in the data for andesites- A and enclaves- B. L-leicester, JD- Joe Devine, SS- (Murphy et al., 1998), BGS- British geological survey, UEA- University of East Anglia, MGU- Mc Gill University.

Lab/Location	Instrument	Samples analyzed by Lab		Phase	Total Number of samples
		An	En		
University of East Anglia	Brucker-AXS S4 Pioneer FluorescenceS spectrometer	1523,1524 M003, M010	M001& M002 M004 to M009 M011 to M019	III	An - 4 En - 17
		1532,1535		IV	An -7
		1537 to 1544	1542, 1566 (a to e) 1587 to 1593	V	An - 12
McGill University, Canada	Philips PW2440 4 kW automated XRF		CM 36 to 38	I	En -3
			CM (26,28,41,51,52,56,58,62,64,65,66,75 A,77)	II	En -13
BGS labs	Spectron X-LAB 2000 ED-XRF	1247/AND (1 to 3)	MVO 1247/MI (1 to 8b)	II	An – 3 En - 9
University of Leicester	PANalytical Axios Advanced PW4400 XRF	40,45 to 57,174 to 242,244 to 332,665 to 725,1003 to 1091	36,49,60 to 63,107 to 115, 663, 675, 679, 682, 1133	I	An – 46 En - 11
		1151,1209 to 1217		II	An - 21
		1323,1330,1350,1387,1445 to 1448		III	An -7
Brown University		94 ,160,171,243	60 to 63, 163 to 165, 488, 530 to 532, 545,551,558, 560 to 564,570 to 572, 580,589	I	An -9 En - 41
		1151A, 1175, 1206, 1208 to1218		II	An - 19
		1323 to 1325, 1327, 1350,1387	1325 (a & b), 1326 (a & b)	III	An – 9 En 4

Table 1 Laboratory and sample information for the XRF data used in this study; An-andesite, En- enclave.

Phase	Total	Plagioclase	Amphibole	Opx	Ti-mag	Qtz	cpx
Murphy et al., 2000 Phase I	45-55	30-35	6-10	2-5	2-4	<0.5	0.5
Murphy et al., 2000 Phase I enclaves		1-5% + xenos	'xenos'	'xenos'		'xenos'	
Devine et al, 1998 Phase I	~40	~30	<6.5	<5	<2	rare	g.mass
Humphreys et al., 2009a*, Phase III	55-63	20-32	3-9.2	1.5-3	0.57-2.58	0-0.76	0.27-1.46
Humphreys et al.,2009a Phase II	33-42	26-32	5-7.5	1.5-3	0.76-1.39	0.05-0.4	0.5-0.66

Table 2 Published modal mineral contents for the first three extrusion phases. Arbitrary distinction between microlites and microphenocryst defined by 100µm, \*Recalculated from point counts in Humphreys et al.,2009a, range shown.



Mineral Phase	Crystal Textures Present	
	Andesite	Enclave
<b>Plagioclase</b>	subhedral –euhedral phenocrysts, zoning (sieved, normal, reverse, patchy and oscillatory)  normally zoned microlites  euhedral, hopper shaped or skeletal	subhedral-euhedral phenocrysts  zoning (sieved, normal, reverse and oscillatory); interpreted as inherited phenocrysts from the andesite  euhedral microphenocrysts  microlites (euhedral, dendritic, acicular or hopper shaped)
<b>Amphibole</b>	anhedral –euhedral phenocrysts  rims (decompression, thermal and resorbed)  rare microlites present in phase II	euhedral-subhedral microphenocrysts  euhedral microlites  Large inherited phenocrysts typically have thermal breakdown textures
<b>Orthopyroxene</b>	euhedral-subhedral phenocrysts  zoning (normal, reverse)  skeletal microlites	euhedral-anhedral microphenocrysts  Large inherited phenocrysts typically have cpx overgrowth rims
<b>Clinopyroxene</b>	euhedral-subhedral microphenocrysts,  zoning (normal; rare oscillatory and sector)  skeletal, normally zoned microlites	subhedral-euhedral microphenocrysts  overgrowths on amphibole rims
<b>Fe-Ti oxides</b>	euhedral-subhedral, unzoned phenocryst  anhedral –subhedral, zoned microphenocrysts  euhedral microlites	euhedral microphenocrysts  euhedral-subhedral microlites
<b>Quartz</b>	Rounded and embayed, sometimes with cpx overgrowth rim	Rounded and embayed with cpx overgrowth rim

Table 3 Mineral phases and associated textures in the andesite and enclave lavas of the current eruption.

Description	PI-PIII pc	PV pc	PI-PIII pr	PIV pr	PV pr	PI-PIII mc	PIV mc	PV mc	PI-PIII mr	PIV mr	mpc	mpr	mr
Host	An	An	An	An	An	An	An	An	An	An	En	En	En
n	35	20	71	64	14	89	35	38	32	19	23	26	25
SiO <sub>2</sub>	53.15	55.28	53.54	53.5	54.5	51.12	51.04	49.62	52.9	51.21	47.94	51.65	49.26
TiO <sub>2</sub>	0.01	0.02	0.02	0.02	0.01	0.02	0.03	0.03	0.02	0.03	0.02	0.03	0.02
Al <sub>2</sub> O <sub>3</sub>	29.4	28.8	28.5	28.9	29	30	30.8	31.62	28.7	30.24	31.92	29.51	31.2
FeO	0.4	0.28	0.5	0.5	0.3	0.64	0.7	0.7	0.6	0.7	0.64	0.66	0.68
MgO	0.04	0.02	0.07	0.08	0.02	0.08	0.08	0.18	0.09	0.07	1.47	0.08	0.08
CaO	12.63	11.27	12	11.8	11.41	13.6	13.8	14.73	12.19	13.6	14.85	13.26	15.1
Na <sub>2</sub> O	4.4	4.94	4.47	4.72	4.9	3.64	3.6	3	4.42	3.7	2.13	3.87	2.91
K <sub>2</sub> O	0.14	0.12	0.16	0.15	0.11	0.11	0.12	0.07	0.12	0.18	0.05	0.12	0.09
Total	100.18	100.72	99.21	99.62	100.18	99.17	100.08	99.86	98.99	99.73	99.02	99.18	99.34
Mean XAn	60.5	55	58.8	57.1	55.6	66.6	67.1	72.71	59.63	66.11	79	64.7	74.2
± 1σ	11	4	10	8	5	8	10	9	7	9	9	9	11

Table 4 Averaged andesite plagioclase phenocryst and microlite microprobe data, comparing compositions from Phases IV and V with the published compositions of Phases I, II and III. pc- phenocryst core, pr - phenocryst rim, mc- microlite core, mr- microlite rim, mpc- microphenocryst core, mpr – microphenocryst rim, An- andesite, En – enlave.

	<b>P1-P3 phx core</b>	<b>P5 core</b>	<b>P1-P3 phx rim</b>	<b>P4 rim</b>	<b>P5 rim</b>	<b>P1-P3 mphx core</b>	<b>P4 mphx core</b>	<b>P5 mphx core</b>
<b>n</b>	<b>108</b>	<b>27</b>	<b>32</b>	<b>7</b>	<b>14</b>	<b>13</b>	<b>4</b>	<b>14</b>
<b>SiO2</b>	47.29	47.14	47.35	47.43	47.35	45.06	48.2	45.7
<b>TiO2</b>	1.46	1.46	1.44	1.44	1.41	1.63	1.46	1.64
<b>Al2O3</b>	7.11	7.32	7.15	7.37	6.94	9.56	6.79	8.36
<b>FeO</b>	14.78	14.91	14.4	14.72	14.61	13.88	14.63	15.5
<b>MnO</b>	0.53	0.51	0.5	0.51	0.53	0.39	0.54	0.48
<b>MgO</b>	13.64	13.69	13.85	13.81	13.8	13.68	13.78	12.96
<b>CaO</b>	10.7	10.71	10.79	10.95	10.79	10.74	10.84	10.72
<b>Na2O</b>	1.36	1.36	1.34	1.36	1.3	1.73	1.26	1.55
<b>K2O</b>	0.19	0.19	0.19	0.2	0.19	0.21	0.17	0.22
<b>Cl</b>	0.11	0.14	0.12	0.13	0.14	0.11	0.13	0.17
<b>Total</b>	97.17	97.42	97.12	97.91	97.06	96.98	97.8	97.3
<b>Mg #</b>	<b>0.48±0.02</b>	<b>0.48±0.02</b>	<b>0.49±0.03</b>	<b>0.48±0.03</b>	<b>0.49±0.02</b>	<b>0.50±0.05</b>	<b>0.49±0.01</b>	<b>0.46±0.02</b>

Table 5a Averaged andesite amphibole compositions by texture and eruption phase.

	<b>P1 en</b>		<b>P2 en</b>		<b>P3 en</b>		<b>P5 en</b>	<b>Mph</b>		<b>Frag</b>	
<b>n</b>	<b>16</b>	$\pm 1\sigma$	<b>11</b>	$\pm 1\sigma$	<b>8</b>	$\pm 1\sigma$	<b>36</b>	<b>9</b>	$\pm 1\sigma$	<b>19</b>	$\pm 1\sigma$
<b>SiO2</b>	42.07	1.75	41.91	1.43	41.15	0.8	41.35	41.69	1.15	42.1	1.34
<b>TiO2</b>	1.74	0.16	1.94	0.13	1.94	0.09	2.00	1.83	0.15	1.92	0.14
<b>Al2O3</b>	12.92	2.12	13.26	1.8	14.16	0.7	14.49	13.5	1.33	12.88	1.63
<b>FeO</b>	13.09	1.37	11.7	1.14	10.28	0.8	10.30	11.89	1.78	11.84	1.43
<b>MnO</b>	0.28	0.16	0.19	0.08	0.15	0.02	0.13	13.77	0.91	14.04	0.78
<b>MgO</b>	13.17	0.92	13.96	0.76	14.81	0.46	15.00	0.2	0.06	0.21	0.09
<b>CaO</b>	11.53	0.32	11.33	0.36	11.62	0.19	11.85	11.2	0.4	11.1	0.52
<b>Na2O</b>	2.21	0.2	2.21	0.21	2.41	0.04	2.42	2.25	0.2	2.22	0.23
<b>K2O</b>	0.2	0.04	0.22	0.02	0.21	0.02	0.25	0.24	0.02	0.21	0.02
<b>Cl</b>	-	-	0.07	0.05	0.05	0.03	0.02	0.06	0.03	0.04	0.03
<b>Tot</b>	97.19		96.79		96.78		97.80	96.63		96.56	
<b>Mg#</b>	<b>0.5</b>	<b>0.04</b>	<b>0.54</b>	<b>0.03</b>	<b>0.59</b>	<b>0.03</b>	<b>0.59</b>	<b>0.54</b>	<b>0.05</b>	<b>0.54</b>	<b>0.04</b>

Table 5b Averaged enclave amphibole compositions from eruption Phases I, II, III and V along side high aluminum andesite hosted microphenocrysts and groundmass fragments. Mphx – microphenocrysts, Frag – groundmass fragments. Phase V data from Plail et al. (this volume)

	<b>P1-P3 phx core</b>	<b>P5 phx core</b>	<b>P1-P3 phx rim</b>	<b>P4 phx rim</b>	<b>P5 phx rim</b>	<b>P1-P3 mic core</b>	<b>P4 mic core</b>	<b>P5 mic core</b>
<b>n</b>	<b>106</b>	<b>15</b>	<b>72</b>	<b>13</b>	<b>8</b>	<b>38</b>	<b>19</b>	<b>12</b>
<b>SiO2</b>	52.37	52.43	52.45	52.44	52.65	52.92	52.7	53.26
<b>TiO2</b>	0.11	0.11	0.12	0.11	0.12	0.2	0.21	0.17
<b>Al2O3</b>	0.59	0.58	0.69	0.64	0.62	1.41	1.24	1.05
<b>FeO</b>	24.18	24.19	23.17	23.68	24.21	19.68	19.92	21.8
<b>MnO</b>	1.57	1.58	1.48	1.53	1.66	0.92	0.97	1.27
<b>MgO</b>	20.08	20	20.61	20.3	20.14	22.67	22.93	21.17
<b>CaO</b>	1	0.95	1.06	1.01	1.02	1.6	1.6	1.3
<b>Na2O</b>	0.01	0.02	0.01	0.02	0.02	0.03	0.04	0.02
<b>Tot</b>	99.93	99.85	99.6	99.72	100.43	99.43	99.61	100.01
<b>En</b>	<b>58.82</b>	<b>59</b>	<b>60.29</b>	<b>59.84</b>	<b>58.82</b>	<b>65.34</b>	<b>65.95</b>	<b>62.15</b>
<b>Fs</b>	<b>39.07</b>	<b>39</b>	<b>37.47</b>	<b>37.86</b>	<b>39.05</b>	<b>31.34</b>	<b>30.75</b>	<b>35.15</b>
<b>Mg#</b>	<b>0.6 ± 0.02</b>	<b>0.6 ± 0.01</b>	<b>0.61 ± 0.03</b>	<b>0.61 ± 0.02</b>	<b>0.6 ± 0.01</b>	<b>0.67 ± 0.05</b>	<b>0.67 ± 0.06</b>	<b>0.63 ± 0.04</b>

Table 6a Averaged Orthopyroxene phenocryst and microlite compositions comparing the andesite crystals of phase IV and V with crystals from phases I, II and III , errors are  $\pm 1\sigma$ , mic – microlites, phx-phenocrysts.

	<b>Opx-Mphx core</b>	<b>Opx-Mphx rim</b>	<b>Rev zoned Opx-Phx rims</b>	<b>Opx Mphx</b>
<b>Host</b>	<b>Andesite</b>	<b>Andesite</b>	<b>Andesite</b>	<b>Enclave</b>
<b>n</b>	<b>12</b>	<b>15</b>	<b>18</b>	<b>18</b>
<b>SiO<sub>2</sub></b>	52.43	52.5	53.35	52.5
<b>TiO<sub>2</sub></b>	0.11	0.16	0.16	0.23
<b>Al<sub>2</sub>O<sub>3</sub></b>	0.65	0.86	1.04	1.33
<b>FeO</b>	23.28	22.55	19.82	21.18
<b>MnO</b>	1.48	1.4	0.93	1.08
<b>MgO</b>	20.35	20.77	23.15	22.02
<b>CaO</b>	0.98	1.23	1.5	1.48
<b>Na<sub>2</sub>O</b>	0.01	0.02	0.02	0.03
<b>Tot</b>	99.3	99.48	99.98	99.84
<b>En</b>	<b>59.7</b>	<b>60.7</b>	<b>65.9</b>	<b>63.6</b>
<b>Fs</b>	<b>38.2</b>	<b>36.8</b>	<b>31</b>	<b>33.3</b>
<b>Mg#</b>	<b>0.61 ± 0.02</b>	<b>0.62 ± 0.03</b>	<b>0.7 ± 0.02</b>	<b>0.64 ± 0.05</b>

Table 6b Averaged compositions of andesite hosted reverse zoned orthopyroxene phenocryst rims along with andesite and enclave microphenocrysts, errors are  $\pm 1\sigma$ , Mphx-microphenocrysts, Phx- phenocrysts.

	P1-P3 Andesite mphx	P5 Andesite mphx	P1-P3 Andesite mic	P4 Andesite mic	P5 Andesite mic	Andesite hosted overgrowths	Enclave mphx
n	29	8	66	23	18	28	24
SiO2	51.22	52.22	51.22	50.71	50.85	50.25	50.5
TiO2	0.45	0.32	0.5	0.63	0.53	0.6	0.62
Al2O3	2.28	1.61	2.88	3.04	2.91	3.61	3.26
FeO	10.51	9.99	10.19	10.18	9.88	9.66	10.83
MnO	0.54	0.63	0.49	0.44	0.47	0.38	0.52
MgO	14.8	14.66	14.53	14.47	14.51	14.49	14.22
CaO	19.06	20.4	18.93	19.65	19.74	19.62	18.99
Na2O	0.23	0.22	0.24	0.27	0.28	0.23	0.27
Total	99.08	100.05	98.97	99.37	99.17	98.84	99.21
Si/Al	22.46	32.43	17.78	16.68	17.47	13.92	15.49
Wo	40.72	42.8	40.75	42.56	42.73	42.6	41.3
En	43.93	42.8	43.52	43.58	43.7	43.7	43.1
Mg#	0.72 ± 0.01	0.72 ± 0.03	0.72 ± 0.02	0.72 ± 0.02	0.72 ± 0.03	0.72 ± 0.03	0.7 ± 0.02

Table 6c Averaged compositions of clinopyroxene microphenocrysts, microlites and overgrowths, errors are  $\pm 1\sigma$ , mic – microlites, mphx- microphenocrysts.

	<b>P1-P3 mph cores</b>	<b>P4 mph cores</b>	<b>P5 mph cores</b>	<b>P1-P3 mph rims</b>	<b>P4 mph rims</b>	<b>P5 mph rims</b>	<b>P1-P3 mic</b>	<b>P4 mic</b>	<b>P5 mic</b>
<b>n</b>	<b>32</b>	<b>9</b>	<b>9</b>	<b>21</b>	<b>15</b>	<b>8</b>	<b>69</b>	<b>27</b>	<b>5</b>
<b>SiO<sub>2</sub></b>	0.09	0.12	0.11	0.11	0.13	0.1	0.38	0.54	0.3
<b>TiO<sub>2</sub></b>	8.4	10.26	8.11	8.27	9.64	8.03	10.69	10.8	7.71
<b>Al<sub>2</sub>O<sub>3</sub></b>	2.04	1.67	1.97	2.19	1.76	1.72	2.02	1.82	1.83
<b>FeO</b>	80.85	81.17	82.27	80.94	81.06	81.98	77.55	79.1	80.6
<b>MnO</b>	0.62	0.58	0.63	0.6	0.62	0.59	0.62	0.67	0.63
<b>MgO</b>	1.27	1.32	1.18	1.16	1.39	1.26	1.15	1.38	1.08
<b>CaO</b>	0.04	0.03	0.04	0.04	0.16	0.08	0.1	0.15	0.09
<b>Total</b>	93.31	95.15	94.32	93.3	94.75	93.77	92.5	94.46	92.23
<b>Usp mol%</b>	<b>25</b>	<b>30</b>	<b>24</b>	<b>25</b>	<b>28</b>	<b>23</b>	<b>33</b>	<b>32</b>	<b>23</b>
<b>± 1σ</b>	5	6	2	4	6	1	9	5	1

Table 7a Averaged andesite titanomagnetite compositions, sorted by eruptive phase and textural type. Usp/Ilm mol% after Stormer (1983), mic – microlites.



	<b>En Mic</b>	<b>En mph</b>	<b>An Ilm</b>	<b>En Ilm</b>
<b>n</b>	<b>22</b>	<b>12</b>	<b>26</b>	<b>8</b>
<b>SiO2</b>	0.39	0.15	0.03	0.03
<b>TiO2</b>	11.99	8.46	42.4	43.5
<b>Al2O3</b>	1.73	2.44	0.2	0.21
<b>FeO</b>	77.49	81.45	51.15	50.1
<b>MnO</b>	0.57	0.59	0.79	0.78
<b>MgO</b>	1.15	1.26	2.19	2.04
<b>CaO</b>	0.13	0.06	0.05	0.05
<b>Total</b>	93.45	94.4	96.81	96.68
<b>Usp/Ilm mol %</b>	<b>36</b>	<b>28</b>	<b>80</b>	<b>83</b>
<b>± 1σ</b>	11	8	3	6

Table 7b Averaged compositions of enclave oxides along with andesite hosted ilmenite.

Andesite	n	SiO2	TiO2	Al2O3	FeO	MgO	CaO	Na2O	K2O	Total	Mg#	Fe/Mg	Ca/Al	Tot alkali	<i>fO2 logunits</i>
<b>Phase 1</b>	<b>81</b>	76.64	0.37	12.15	1.72	0.23	1.81	3.51	2.84	99.34	0.1	7.5	0.14	6.35	NNO +1- +1.2
$\pm \sigma$		<b>2.2</b>	<b>0.09</b>	<b>1.3</b>	<b>0.5</b>	<b>0.26</b>	<b>1</b>	<b>0.6</b>	<b>1.4</b>	<b>1.1</b>	<b>0.07</b>		<b>0.07</b>	<b>1.2</b>	
<b>Phase 2</b>	<b>21</b>	78.22	0.4	11.09	1.37	0.17	0.89	3	4.56	99.6	0.1	8	0.08	7.56	NNO + 0.5- +1.3
$\pm \sigma$		<b>2</b>	<b>0.19</b>	<b>0.45</b>	<b>0.5</b>	<b>0.09</b>	<b>0.6</b>	<b>0.7</b>	<b>1.5</b>	<b>1.2</b>	<b>0.05</b>		<b>0.05</b>	<b>1.1</b>	
<b>Phase 3</b>	<b>40</b>	75.71	0.35	11.64	1.8	0.2	1.28	3.77	3.85	98.9	0.1	9	0.11	7.7	NNO+ 0.5- +1.4
$\pm \sigma$		<b>2.2</b>	<b>0.14</b>	<b>1.45</b>	<b>0.6</b>	<b>0.14</b>	<b>0.9</b>	<b>0.7</b>	<b>1.3</b>	<b>1.3</b>	<b>0.05</b>		<b>0.06</b>	<b>1.3</b>	
<b>Phase 4</b>	<b>14</b>	78.25	0.3	11.26	1.78	0.25	1.28	3.87	2.64	99.8	0.12	7	0.11	6.5	NNO+ 0.9- +1.1
$\pm \sigma$		<b>1.12</b>	<b>0.12</b>	<b>0.5</b>	<b>0.4</b>	<b>0.18</b>	<b>0.3</b>	<b>0.2</b>	<b>0.2</b>	<b>1.4</b>	<b>0.06</b>		<b>0.02</b>	<b>0.3</b>	
<b>Phase 5</b>	<b>13</b>	76.09	0.27	11.8	1.34	0.14	1.46	3.04	2.44	97	0.1	9.6	0.12	5.5	NNO +1.4
$\pm \sigma$		<b>2</b>	<b>0.07</b>	<b>1.4</b>	<b>0.3</b>	<b>0.1</b>	<b>0.9</b>	<b>0.6</b>	<b>0.8</b>	<b>2.2</b>	<b>0.05</b>		<b>0.06</b>	<b>1</b>	
<b>Enclave</b>															
<b>Phase 1</b>	<b>4</b>	78.26	0.44	11.67	1.39	0.1	1.59	3.28	3.21	100.01	0.07	13.9	0.14	6.5	
$\pm \sigma$		<b>2.4</b>	<b>0.12</b>	<b>0.18</b>	<b>0.8</b>	<b>0.08</b>	<b>1.11</b>	<b>1.06</b>	<b>3.1</b>	<b>0.01</b>	<b>0.02</b>		<b>0.1</b>	<b>2.3</b>	
<b>Phase 2</b>	<b>10</b>	74.7	0.41	12.3	1.8	0.11	1.24	3.6	4.6	98.9	0.06	16.6	0.1	8.19	
$\pm \sigma$		<b>1.9</b>	<b>0.1</b>	<b>1.4</b>	<b>0.26</b>	<b>0.03</b>	<b>0.9</b>	<b>0.6</b>	<b>0.8</b>	<b>1.7</b>	<b>0.01</b>		<b>0.06</b>	<b>0.98</b>	
<b>Phase 4</b>	<b>4</b>	78.17	0.4	11.22	2.12	0.34	1.36	3.62	2.9	100.3	0.13	6.2	0.12	6.5	
$\pm \sigma$		<b>0.6</b>	<b>0.19</b>	<b>0.5</b>	<b>0.15</b>	<b>0.26</b>	<b>0.3</b>	<b>0.3</b>	<b>0.3</b>	<b>0.4</b>	<b>0.08</b>		<b>0.03</b>	<b>0.32</b>	

Table 8 Averaged microprobe glass compositions for andesites and enclaves, along with log  $f_{O2}$  values from touching ilmenite–magnetite pairs.

Andesite	n	SiO2	TiO2	Al2O3	FeO	MnO	MgO	CaO	Na2O	K2O	P2O5	Tot	Fe/Mg	Ca/Al	Tot alk
Phase 1	55	59.22	0.61	17.81	7.32	0.18	2.87	7.49	3.56	0.78	0.15	99.99	2.56	0.42	4.35
± σ		<b>0.82</b>	<b>0.04</b>	<b>0.36</b>	<b>0.39</b>	<b>0.02</b>	<b>0.19</b>	<b>0.24</b>	<b>0.18</b>	<b>0.08</b>	<b>0.01</b>	<b>0.1</b>	<b>0.1</b>	<b>0.01</b>	<b>0.22</b>
Phase 2	42	58.6	0.63	17.86	7.14	0.18	2.81	7.87	3.77	0.82	0.16	99.83	2.55	0.44	4.59
± σ		<b>1.07</b>	<b>0.05</b>	<b>0.35</b>	<b>0.61</b>	<b>0.02</b>	<b>0.27</b>	<b>0.38</b>	<b>0.16</b>	<b>0.06</b>	<b>0.01</b>	<b>0.32</b>	<b>0.17</b>	<b>0.02</b>	<b>0.19</b>
Phase 3	17	58.96	0.64	17.92	6.56	0.17	2.85	7.63	3.53	0.82	0.14	99.19	2.32	0.43	4.35
± σ		<b>1.2</b>	<b>0.04</b>	<b>0.38</b>	<b>0.5</b>	<b>0.02</b>	<b>0.33</b>	<b>0.4</b>	<b>0.23</b>	<b>0.06</b>	<b>0.02</b>	<b>0.61</b>	<b>0.18</b>	<b>0.02</b>	<b>0.24</b>
Phase 4	7	58.59	0.63	17.95	7.41	0.18	3.14	7.67	3.52	0.8	0.14	100.03	2.37	0.43	4.33
± σ		<b>0.86</b>	<b>0.02</b>	<b>0.18</b>	<b>0.21</b>	<b>0.01</b>	<b>0.22</b>	<b>0.29</b>	<b>0.1</b>	<b>0.04</b>	<b>-</b>	<b>0.31</b>	<b>0.10</b>	<b>0.01</b>	<b>0.13</b>
Phase 5	13	59.91	0.59	17.68	7.08	0.18	2.76	7.12	3.56	0.86	0.14	99.81	2.58	0.4	4.42
± σ		<b>1.11</b>	<b>0.03</b>	<b>0.3</b>	<b>0.28</b>	<b>-</b>	<b>0.27</b>	<b>0.4</b>	<b>0.14</b>	<b>0.06</b>	<b>0.01</b>	<b>0.18</b>	<b>0.16</b>	<b>0.02</b>	<b>0.19</b>
Enclave															
Phase 1	55	52.36	0.84	19.38	9.61	0.2	4.26	9.88	2.76	0.51	0.14	99.95	2.27	0.51	3.27
± σ		<b>1.57</b>	<b>0.08</b>	<b>0.54</b>	<b>0.63</b>	<b>0.02</b>	<b>0.43</b>	<b>0.6</b>	<b>0.36</b>	<b>0.12</b>	<b>0.02</b>	<b>0.23</b>	<b>0.22</b>	<b>0.03</b>	<b>0.42</b>
Phase 2	22	53.13	0.8	19.27	9.31	0.21	4.2	9.63	3.12	0.55	0.13	100.34	2.25	0.5	3.66
± σ		<b>1.71</b>	<b>0.05</b>	<b>0.56</b>	<b>0.47</b>	<b>0.02</b>	<b>0.58</b>	<b>0.66</b>	<b>0.3</b>	<b>0.11</b>	<b>0.02</b>	<b>0.35</b>	<b>0.26</b>	<b>0.02</b>	<b>0.33</b>
Phase 3	22	51.89	0.81	19.59	8.44	0.18	4.68	9.77	2.82	0.5	0.11	98.7	1.83	0.5	3.32
± σ		<b>1.68</b>	<b>0.07</b>	<b>0.47</b>	<b>0.4</b>	<b>0.01</b>	<b>0.58</b>	<b>0.69</b>	<b>0.25</b>	<b>0.07</b>	<b>0.02</b>	<b>0.66</b>	<b>0.26</b>	<b>0.03</b>	<b>0.29</b>
Phase 5	12	54	0.75	19.04	8.45	0.18	4.13	9.26	3.2	0.56	0.12	99.69	2.06	0.49	3.76
± σ		<b>0.96</b>	<b>0.03</b>	<b>0.34</b>	<b>0.41</b>	<b>0.02</b>	<b>0.34</b>	<b>0.46</b>	<b>0.21</b>	<b>0.06</b>	<b>0.02</b>	<b>0.23</b>	<b>0.23</b>	<b>0.02</b>	<b>0.23</b>

Table 9 Averaged bulk rock major element compositions for the andesite and enclaves of the different eruption phases.

Andesite	n	Sc	V	Rb	Sr	Y	Zr	Ba	Zr/Rb	Zr/Ba	Zr/Ti	Ba/Rb	Ba/K
Phase 1	55	16.61	106.23	15.23	272.37	24.31	101.57	225.16	6.8	0.45	161.77	15.04	273.18
± $\sigma$		<b>2.71</b>	<b>15.84</b>	<b>2.42</b>	<b>14.11</b>	<b>1.37</b>	<b>6.66</b>	<b>25.44</b>	<b>0.97</b>	<b>0.03</b>	<b>16.21</b>	<b>2.19</b>	<b>21.95</b>
Phase 2	31	17.19	117.58	15.23	272.37	24.31	101.57	225.16	6.8	0.45	161.77	15.04	273.18
± $\sigma$		<b>1.35</b>	<b>18.7</b>	<b>2.42</b>	<b>14.11</b>	<b>1.37</b>	<b>6.66</b>	<b>25.44</b>	<b>0.97</b>	<b>0.03</b>	<b>16.21</b>	<b>2.19</b>	<b>21.95</b>
Phase 3	6	14.25	115.63	16.83	261.5	21.33	97.13	212.17	5.8	0.46	145.83	12.57	251.19
± $\sigma$		<b>2.75</b>	<b>19.68</b>	<b>1.83</b>	<b>8.38</b>	<b>1.21</b>	<b>8.17</b>	<b>34.13</b>	<b>0.35</b>	<b>0.05</b>	<b>15.62</b>	<b>1.15</b>	<b>32.45</b>
Phase 4	10	15.71	140.71	16	255.86	20.86	93.57	169.71	5.85	0.55	148.53	10.6	211.25
± $\sigma$		<b>2.21</b>	<b>10.34</b>	<b>0.58</b>	<b>2.12</b>	<b>0.9</b>	<b>3.74</b>	<b>12.32</b>	<b>0.15</b>	<b>0.03</b>	<b>11.13</b>	<b>0.63</b>	<b>8.88</b>
Phase 5	6	13.20	117.8	16.8	258.2	21.4	98.2	192.6	5.86	0.51	168.42	11.44	226.55
± $\sigma$		<b>1.64</b>	<b>17.85</b>	<b>1.3</b>	<b>0.84</b>	<b>0.55</b>	<b>4.32</b>	<b>23.01</b>	<b>0.26</b>	<b>0.04</b>	<b>17.75</b>	<b>0.64</b>	<b>10.24</b>
Enclave													
Phase 1	18	21.33	174.88	10.61	275.22	23.04	69.56	136.78	7.42	0.55	88.45	13.68	247.66
± $\sigma$		<b>2.64</b>	<b>24.64</b>	<b>3.42</b>	<b>11.95</b>	<b>2.25</b>	<b>8.45</b>	<b>39.84</b>	<b>3.18</b>	<b>0.15</b>	<b>13.57</b>	<b>4.28</b>	<b>66.31</b>
Phase 2	13		200.69	11.08	275.74	22.66	68.59	115.69	6.44	0.65	85.1	10.45	204.53
± $\sigma$			<b>34.33</b>	<b>2.54</b>	<b>10.45</b>	<b>4.47</b>	<b>7.82</b>	<b>39.43</b>	<b>1.42</b>	<b>0.2</b>	<b>13.63</b>	<b>2.37</b>	<b>39.99</b>
Phase 3	21	25.41	227.77	9.84	267.24	20.43	63.14	77.76	6.69	0.97	77.85	7.92	153.4
± $\sigma$		<b>5.24</b>	<b>36.54</b>	<b>1.71</b>	<b>10.06</b>	<b>1.83</b>	<b>14.87</b>	<b>30.95</b>	<b>1.66</b>	<b>0.49</b>	<b>19.94</b>	<b>2.43</b>	<b>54.68</b>
Phase 5	12	21.25	191.58	11.55	271.92	22.33	71.50	104.17	6.34	0.69	95.91	9.18	185.56
± $\sigma$		<b>2.8</b>	<b>27.5</b>	<b>1.21</b>	<b>8.27</b>	<b>4.85</b>	<b>11.49</b>	<b>18.3</b>	<b>0.59</b>	<b>0.09</b>	<b>19.53</b>	<b>1.08</b>	<b>20.06</b>

Table 10 Averaged bulk rock trace element for andesites and enclaves of the different eruption phases.

<b>Tmin °C</b>	<b>Tmax °C</b>	<b>Avg °C</b>	<b>Stdev ± °C</b>	<b>no. analyses</b>	<b>Method</b>	<b>Phase texture</b>
824	965	866	30	17	Single-pyroxene QUILF method	Opx/Microphenocryst cores
845	895	869	15	14	Single-pyroxene QUILF method	Opx/Microphenocryst rims
1018	1032	1025	6	4	Single-pyroxene QUILF method	Opx/Microphenocryst rims (showing heated textures)
785	938	851	23	77	Single-pyroxene QUILF method	Opx/Phenocryst cores
799	1028	878	65	65	Single-pyroxene QUILF method	Opx/Phenocryst rims
826	1101	988	82	26	Single-pyroxene QUILF method	Opx/Zoned phenocryst rims
903	1305	1070	106	16	Single-pyroxene QUILF method	Opx/Mafic inclusions
791	809			4	2-oxides QUILF (Andersen et al. 1993)	Ox/Included in minerals or in crystal clots
958	1017			3	2-oxides QUILF (Andersen et al. 1993)	Ox/Zoned microphenocrysts or microlites
1074	1196	1109	45	5	2-pyroxene QUILF (Andersen et al. 1993)	2Px/Mafic inclusion pairs
903	1142	1021	78	15	2-pyroxene QUILF (Andersen et al. 1993)	2Px/Microlite pairs
804	890	833	24	10	Hb-plag equilibria Holland & Blundy	Hb-plg Andesite pairs (using ed-ri thermometer, 200 MPa)
849	947	894	34	9	Hb-plag equilibria Holland & Blundy	Hb-plg Mafic inclusion pairs (using ed-ri thermometer, 200 MPa)
821	1100	920	70	36	Plag-melt	Andesite hosted microlites (XAn 0.45-0.84)
1097	1145	1110	35	19	Cpx-melt	Enclave microlites/microphenocryst rims

Table 11 Temperature and Pressure estimates for the eruptive products obtained using a number of different techniques.

<b>Initial</b>	<b>Final</b>	<b>amph wt%</b>	<b>Plag wt%</b>	<b>Opx wt%</b>	<b>Cpx wt%</b>	<b>Ox wt%</b>	<b>R<sup>2</sup></b>
Phase I Low Fe andesite	Phase I High Fe andesite	+11	-4	+10	-16	-4	0.15
Phase II Low Fe andesite	Phase II High Fe andesite	-	+16	+6	+3	+4	0.025
Phase III Low Fe andesite	Phase III High Fe andesite	-	+9	+1	+5	+3	0.25

Table 12 Intra- phase andesite mass balance calculations for addition of enclave crystals, weight % values are relative to initial magma compositions.